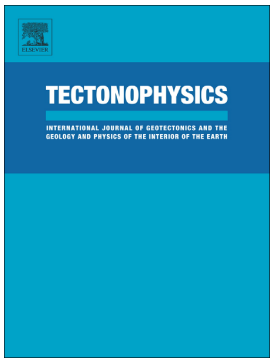

Subsurface characterization of quaternary scarps and their possible connection to main structures of the western margin of Precordillera, San Juan, Argentina

V. Gisel Peri, Augusto E. Rapalini, Pablo Pérez, Pablo Franceschinis, M. Flavia Leiva, Sabrina Y. Fazzito, José M. Cortés

PII: S0040-1951(20)30225-0

DOI: https://doi.org/10.1016/j.tecto.2020.228542

Reference: TECTO 228542

To appear in: *Tectonophysics*

Received date: 14 July 2019

Revised date: 30 April 2020

Accepted date: 16 June 2020

Please cite this article as: V.G. Peri, A.E. Rapalini, P. Pérez, et al., Subsurface characterization of quaternary scarps and their possible connection to main structures of the western margin of Precordillera, San Juan, Argentina, *Tectonophysics* (2019), https://doi.org/10.1016/j.tecto.2020.228542

SUBSURFACE CHARACTERIZATION OF QUATERNARY SCARPS AND THEIR POSSIBLE CONNECTION TO MAIN STRUCTURES OF THE WESTERN MARGIN OF PRECORDILLERA, SAN JUAN, ARGENTINA

V. Gisel Peri[a], Augusto E. Rapalini[a], Pablo Pérez[b], Pablo Franceschinis[a], M. Flavia Leiva[c], Sabrina Y. Fazzito[a], José M. Cortés[a]

a. Instituto de Geociencias Básicas Aplicadas y Ambientales de Buenos Aires (IGEBA), Universidad de Buenos Aires, CONICET, Intendente Güiraldes 2160, Pabellón II, Piso 1, Ciudad Universitaria, Ciudad Autónoma de Buenos Aires, CP1428, Argentina. vgiselperi@gmail.com; rapalini@gl.fcen.uba.ar; pablo.franceschinis2@gmail.com; sabrinafazzito@gl.fcen.uba.ar; josemacortes@yahoo.com.

b. Instituto de Geología y Recursos Minerales, Servicio Geológico Minero Argentino (SEGEMAR), Av. General Paz 5445, Parque Tecnológico Miguelete, Edificio 25. San Martín, B1650 WAB, Buenos Aires, Argentina. pablofp92@gmail.com.

c. Instituto Geofísico Sismológico Volponi (IGSV), Universidad Nacional de San Juan, CONICET, Ruta 12 KM 17, Rivadavia, J5402CWH, San Juan, Argentina. mariaflavialeiva@gmail.com.

CORRESPONDING AUTHOR

V. Gisel Peri, vgiselperi@gmail.com

HIGHLIGHTS

1. Quaternary analysis of the western piedmont of Sierra del Tigre is presented.
2. Topographic and geoelectrical surveys were done across fault and fold scarps.
3. Three geoelectrical levels and subvertical conductive zones were identified.
4. A frontal splay of the backthrust of the Sierra del Tigre was inferred.
5. Quaternay compressive deformation has originated the piedmont deformation belt.

ABSTRACT

The El Tigre fault provides a significant example of Pliocene-Quaternary tectonic activity at the West of Precordillera, receiving considerable attention in the last years. However, longitudinal thrusts of the nearest Sierra del Tigre and a minor piedmont deformation belt identified in its western piedmont are still poorly understood. The present work comprised a detailed map of the geomorphological features of tectonic origin and Quaternary alluvial fan terraces located between the Sierra del Tigre and the El Tigre fault. Several topographic and geoelectrical profiles across minor fault and fold scarps were surveyed to define the displacement scarps, the geological structure geometries at subsurface and their relationship with main structures. Geoelectrical models allowed us to recognize three geoelectrical levels: A (> 200-300 Ω.m) correlated to Pleistocene alluvial fan terraces Q4 and Q3; B (ranging from 50-300/450 Ω.m), under level A and correlated to the Neogene substratum (Rodeo Formation); C (< 30-40 Ω.m) intercalated in level B, conforming aquifers (20 and 40 m deep) within the Neogene substratum. Subvertical conductive zones (10-40 Ω.m) were correlated to high angle (~60°-80°) reverse faults, which are associated with open anticlines and synclines that affect the Quaternary levels and the Neogene substratum. The structural style interpreted here allows us to conclude that the main piedmont thrust is a frontal splay of the backthrust of the Sierra del Tigre with western vergence. A better connection to the compressive deformation component, which uplifts the range, instead of to the strike-slip deformation component of the El Tigre Fault is demonstrated. This tectonic propagation probably happens during Middle-Upper Pleistocene to Holocene. The observations show that minor deformation belt is subjected to piedmont compressive movements while the El Tigre Fault absorbs the strike-slip movements, so a local partition of the deformation in the western margin of Precordillera probably happens during Quaternary.

KEYWORDS: *Electrical Resistivity Tomography, Neotectonics, Morphotectonics, Argentine Precordillera, El Tigre Fault.*

1. INTRODUCTION

The Andean foreland of Argentina (Figure 1) at the latitude of the Pampean flat-slab segment (30°-32°S; Anderson *et al.*, 2007; Cahill and Isacks 1992) concentrates most of the deformation and shortening of the region. The last significant tectonic phase at the western margin of South America

that produced a major uplift of the main Andes occurred during the Miocene (Ramos, 2009). Afterward, the deformation migrated eastward due to of shallowing of the subduction zone (Figure 1a), uplifting the foreland and leading to the present-day configuration of the Precordillera and its broken foreland (Figure 1b). The highest crustal seismicity of the southern Central Andes is located here, as can be inferred from historically and instrumentally recorded earthquakes (Alvarado and Ramos, 2011; Alvarado *et al.*, 2007; Smalley and Isacks, 1987, 1990; Smalley *et al.*, 1993; www.inpres.gov.ar, accessed June 2019) and from structural and geomorphological evidence (Casa *et al.*, 2014; Costa *et al.*, 2006, 2015a). The present frontal deformation zone is located at the eastern margin of the Precordillera (Figure 1b) with most Quaternary active contractional structures (Bastías, 1985; Brooks *et al.*, 2003; Casa *et al.*, 2014; Cortés *et al.*, 1999, Costa *et al.*, 2000a, b 2006, 2015a; Meigs *et al.*, 2006; Rockwell *et al.*, 2014; Schmidt *et al.*, 2011; Siame *et al.*, 2002, 2005, 2006; Vergés *et al.*, 2007). Moreover, at the Western and Southern Precordillera (Figures 1b and c), several Quaternary-active structures have been reported (Cortés *et al.*, 2015; Fazzito *et al.*, 2013; Terrizzano *et al.*, 2012). The El Tigre fault (Figures 1b, c and 2) constitutes a remarkable Pliocene-Quaternary strike-slip fault of 120 km long and an N-S trend that disrupts Pleistocene alluvial fan terraces located at the western piedmont of the Precordillera. Its almost pure strike-slip displacement is well registered at the southern segment of this fault (Siame *et al.*, 1997a, b; Figure 2a) while a vertical component is better observed at its central segment (Bastías *et al.*, 1984; Siame, 1998, Fazzito *et al.*, 2013, 2016). The El Tigre fault provides one significant example of Pliocene-Quaternary activity (Bastías and Bastías 1987; Cortés *et al.* 1999; Fazzito *et al.*, 2013, 2016; INPRES, 1982; Siame *et al.*, 1997a, b, 2006) at the west of Precordillera.

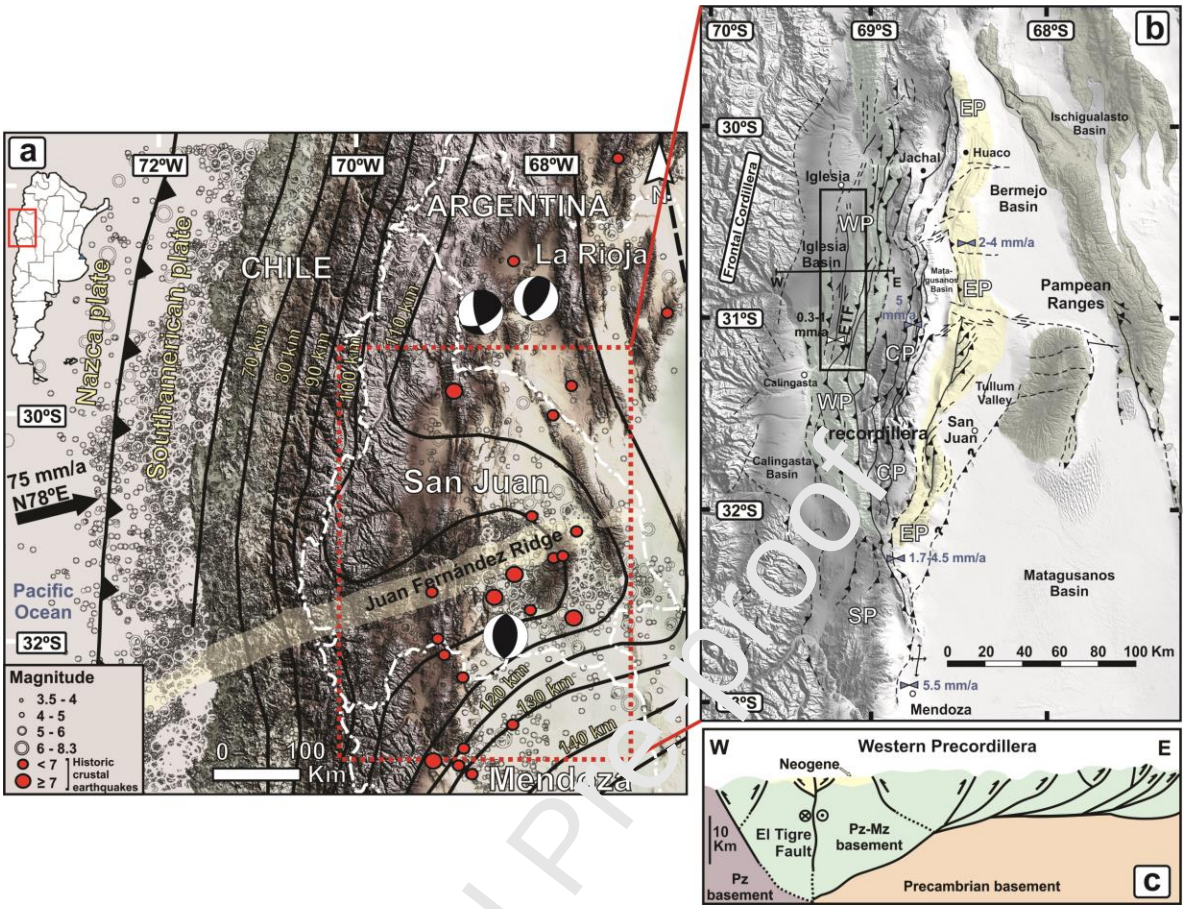

Figure 1. Geological setting. a) Pampean flat-slab segment. The continuous black lines represent contour slab deep. The crustal seismicity of the area is shown in gray circles, historical crustal earthquakes are shown in red circles (Alvarado and Ramos, 2011) and focal mechanisms are also presented (Siame *et al.*, 2005; Alvarado and Ramos, 2011). The dashed red box shows the location of figure b. b) Main morphotectonic units: Precordillera (CP: Central Precordillera, EP: Eastern Precordillera, SP: Southern Precordillera, WP: Western Precordillera), Iglesia-Calingasta basin, Pampean Ranges. Main structures as the El Tigre fault (ETF), thrusts, and backthrusts are also plotted. Shortening rates are shown (see text). The black box shows the location of figure 2a. c) Schematic structural cross-section located at figure b. **3-COLUMNS**

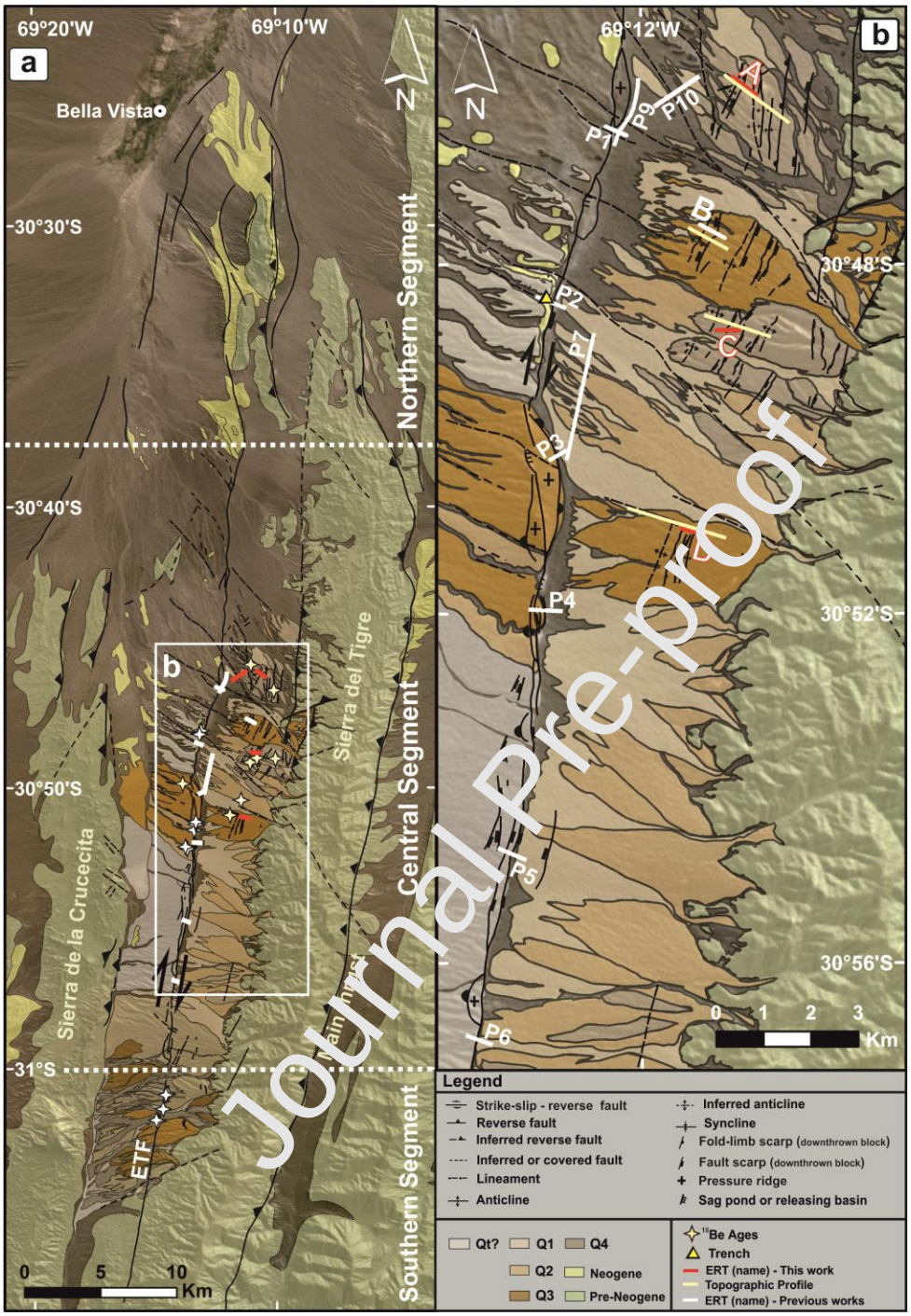

Figure 2. Local geological setting and location of ERTs. a) Geological map of the western piedmont of Sierra del Tigre. The Sierra del Tigre and Sierra de la Crucecita, main structures and segments of the El Tigre Fault (ETF) are illustrated. Insets show the location of figure b. Sites of surface cosmogenic dating by Peri *et al.* (2018; *under review*) and Siame *et al.* (1997a, b) are indicated as yellow and white stars, respectively. b) A detail of the study area is shown with geomorphological features of tectonic origin on the Quaternary alluvial fan terraces. Location of a previous ERTs study (white lines; Fazzito *et al.*, 2013) and for this contribution (red lines). Topographic cross-sections are plotted as yellow lines**. 2-COLUMNS**

Although the El Tigre Fault has received significant attention in the last two decades by several research groups, minor piedmont deformation identified in the eastern hanging wall of this fault, is still poorly understood (Figures 2a and b). At the surface, the eastern hanging wall of El Tigre Fault is formed by dissected and undissected Quaternary alluvial fans that were deformed by several NNE-SSW trending fault and fold scarps (Figure 2). East- and west-facing scarps are present, although natural transversal sections to observe the related underground structures are absent. Previous geoelectrical surveys in the area suggest the presence of high angle east-dipping covered reverse faults (Fazzito *et al.*, 2013) associated with some of these minor fault scarps. The geometry and kinematics of these covered structures must be determined in order to understand how these minor piedmont scarps are related to the main structures of the western margin of Precordillera, such as the El Tigre fault and the thrusts of the Western Precordillera. This knowledge will improve our understanding of the Andean orogenic processes and their seismic potential in the region. The electrical resistivity tomography (ERT) is a well tested and documented geophysical methodology of investigation of the shallow subsurface (*e.g.*, Sharma, 1997). Its application to locate and geometrically characterize faults and other structures with neotectonic activity has proven successful in many investigations (Bufford *et al.*, 2012; Caputo *et al.,* 2003, 2007; Colella *et al.*, 2004; Fazzito *et al.,* 2009, 2013; Nguyen *et al.*, 2005, 2007; Nivière *et al.*, 2008; Pánek *et al.*, 2011; Peri *et al.*, 2017; Rizzo *et al.,* 2004, 2019; Terrizzano *et al.,* 2010, 2012; Wise *et al.,* 2003). The ERT allows to characterize the subsurface resistivity distribution and thus to recognize geoelectrical layers and discontinuities up to around one to two hundred meter depths, depending on the geometrical array used and the electric current introduced in the ground. It has been applied rather successfully in the study of neotectonic structures of the Southern Precordillera (Terrizzano *et al.*, 2010, 2012) as well as the western margin of the Precordillera (Fazzitto *et al.*, 2009, 2013; Peri *et al.*, 2017).

In order to investigate the subsurface structures related to the piedmont deformation at the western margin of the Precordillera and to analyze their structural style and possible association with the main structures of the area as El Tigre fault and longitudinal thrusts of the large mountain blocks (Figure 2), we surveyed five sections across piedmont fault and fold scarps. The dipole-dipole and Wenner-Schlumberger arrays were applied at the north, central, and southern sectors of the Sierra del Tigre western piedmont combining the geophysical studies with topographic and geomorphological quantification scarps displacements. The results obtained were analyzed

together with a previous testing survey across some of these scarps presented by Fazzito *et al.* (2013).

2. GEOLOGICAL SETTING

Since the middle to late Miocene, subduction of the Nazca plate beneath the South American plate has developed a flat-slab segment at latitudes between 30° S and 32° S (Figures 1a and b) (Anderson *et al.*, 2007; Cahill and Isacks, 1992; Gutscher *et al.*, 2000; Ramos *et al.*, 1996, 2002). Significant deformation near the continental margin in the Andean Cordillera (Ramos *et al.*, 2002; Ramos, 2009) was produced and horizontal shortening has been propagated by the migration of deformation toward the Andean foreland of Argentina. Consequently, the highest and most extensive crustal seismicity of the southern Central Andes and whole Argentina is recorded here (Figure 1a; Alvarado and Ramos, 2011; Alvarado *et al.* 2007; Smalley and Isacks 1987, 1990; Smalley *et al.* 1993; www.inpres.gov.ar, accessed June 2019). This deformation raised a series of morphotectonic units: the Frontal Cordillera, the Calingasta-Iglesia Valley, the Precordillera, and the Pampean Ranges, from west to east, respectively (Figure 1b). The current Andean frontal deformation zone is located along the eastern margin of the Precordillera, in a narrow north-south belt, where Quaternary-active contractional structures are concentrated (Bastías *et al.*, 1984; Brooks *et al.*, 2003, Cortés *et al.*, 1999; Costa *et al.*, 2000a, b, 2006, 2015a, b; Casa *et al.*, 2014; Meigs *et al.*, 2006; Rockwell *et al.*, 2014; Schmidt *et al.*, 2011; Siame *et al.*, 2002, 2005, 2006; Vergés *et al.*, 2007). However, at the Western and Southern Precordillera (Figures 1b and c), several Quaternary-active structures have been reported (Cortés *et al.*, 2015; Fazzito *et al.*, 2013; Terrizzano *et al.*, 2013). From regional GPS survey and models, the changes in the crustal velocity field are concentrated between the Precordillera and the Pampean Ranges at estimated rates of ~2–4 mm/a (Kendrick *et al.*, 2003, 2006), and an east-west shortening of 4.5 ± 1.7 mm/a (Brooks *et al.*, 2003). Shortening rates in the Pampean flat-slab segment over a geological timescale of millions of years (Allmendinger *et al.*, 1990; Giambiagi and Ramos, 2002; Jordan *et al.*, 1993; Ramos *et al.*, 2004; Vergés *et al.*, 2007; Zapata and Allmendinger, 1996) has been roughly constant and remarkably similar to the rates measured on millennial and decadal timescales. Still, long- (million years time scale), intermediate- (millennial time scale), and short-term (decadal time scale) rates must be discriminated to understand how the upper crustal deformation is accommodated through

individual structures of the Andean orogenic processes and improve our knowledge about their seismic potential.

The study area is located between the Precordillera and the Calingasta-Iglesia Valley (Figure 1b), in the San Juan province of Argentina. The Precordillera represented the Andean foreland during Neogene and recorded the deformational and depositional history of the last ~15-13 Ma since uplift started around such time (Allmendinger and Judge, 2014; Levina *et al.* 2014; Suriano *et al.*, 2017; Walcek and Hoke, 2012). The Precordillera (30° - 32° S) constitutes a north-trending 400 km long and 80 km wide fold-and-thrust belt off, which is subdivided into four morphotectonic subunits: Western, Central, Eastern, and Southern Precordillera (Figure 1b; Baldis *et al.* 1982; Cortés *et al.*, 2005b; Ortiz and Zambrano 1981). The Western and Central Precordillera conform a ~NNE trending thin-skinned fold-and-thrust belt with tectonic vergence towards the East and a detachment zone at 10-15 km depth (Allmendinger *et al.* 1990; Cristallini and Ramos, 2000; Jordan *et al.* 1993; von Gosen 1992). Meanwhile, the Eastern Precordillera conforms a ~NNE thick-skinned fold-and-thrust belt with western tectonic vergence (Figure 1c). Into the Precordillera (30° - 32° S) Quaternary ruptures are the product of both reactivated and new thrusts oblique or longitudinal to the mountain front faults. Piedmont fold and fault scarps on alluvial sediments are common in the intermontane basins (Bastías *et al.*, 1990; Cortés *et al.,* 1999; Costa *et al.,* 2000a). Most of the evidence of neotectonic deformation in the Andean foreland is concentrated along the eastern flank of the Precordillera, between 31° and 34° S (Cortés *et al.*, 2014; Costa *et al.*, 2006, 2015a). However, evidence of neotectonic activity has also been reported at its western margin. Especially at the western margin of Southern Precordillera (Figure 1b; Basile, 2004; Cortés and Cegarra 2004; Cortés *et al.*, 2005a, b, c, 2006; Perrizzano *et al.*, 2012; Vallejo, 2004; Yamin, 2007) and at Western Precordillera where the main Quaternary structure is the El Tigre fault (Figures 1b and c) that is located in a Neogene intermountain tectonic depression, which to the north is part of the called Calingasta-Iglesia Valley (Figure 1b). This 300 km long and 30 km wide tectonic depression (Beer *et al.*, 1990) was filled by a sequence up to 3.5 km thick in its center made up by Neogene pyroclastics, andesites, and clastic sediments, the Rodeo Formation, which constitute synorogenic deposits associated with the uplift of both, the Frontal Cordillera and the Precordillera. The Neogene Rodeo Formation (Furque, 1979; Wetten, 1975a, b) is divided by Alonso (2011) into the Lomas del Campanario Member (pyroclastic lithology) integrated by four Facies Associations, and the Las Flores Member (epiclastic lithology) integrated by six Facies Associations. An upper Miocene (9.5 ± 0.2 Ma to 11.1 ± 0.3 Ma; Alonso, 2011) to Pliocene (~4 Ma; Johnson *et al.*, 1987; Jordan *et al.*, 1993)

age was assigned by Ar-Ar and U-Pb dating to the lower Lomas del Campanario Member. The Calingasta-Iglesia Valley is interpreted as a piggyback basin that was developed simultaneously with the eastward progress of the Precordilleran thrusts (Beer *et al.*, 1990; Jordan *et al.*, 1993). The infilled sequence was capped by sediments of Quaternary alluvial fans (Furque, 1979; Bastías, 1985; Peri *et al.*, 2017, 2018; Perucca and Martos 2009; Siame *et al.*, 1997a, b), and playa deposits were observed in the lowest part of the tectonic depression, constituting the local base levels of the ephemeral rivers (Perucca and Martos, 2012). Inselbergs and ridges of the Paleozoic basement were raised above the plain, with heights between a few tens up to 200-300 meters.

The tectonic depression where the El Tigre fault is located is flanked by the Sierra del Tigre to the east and by the Sierra de La Crucecita to the west (Figure 2a), which constitute a part of the Western Precordillera and were uplifted by eastern vergence thrusts (Cardó and Díaz 2005). The Sierra del Tigre has developed a prominent NNE-SSW trending backthrust with western vergence and represented by a conspicuous rectilinear trace at the mountain-piedmont union, suggesting a Quaternary tectonic activity (Figures 2a and b). Other regional structures in the study area are ~NW-SE to NNW-SSE lineaments and inferred fault trace (Figure 2a; Fazzito *et al.*, 2013; Peri *et al.*, 2017) that have been associated to the rejuvenation of the bedrock basement. These old structures have influenced the evolution, kinematics and segmentation of the El Tigre fault (Fazzito *et al.* 2013, 2016), which provides one significant example of Pliocene-Quaternary activity (Bastías and Bastías 1987; Cortés *et al*. 1999; INPRES 1982; Siame *et al*., 1997a, b, 2006) at the western margin of Precordillera. Siame *et al.* (2006) suggested that at 30° S both the Calingasta-Iglesia Valley and the Precordillera fold-and-thrust belt can be interpreted as a part of a crustal-scale transpressive zone, whose dextral strike-slip component is occurred mainly along the El Tigre Fault zone. Morphotectonic features reveal the Quaternary activity of this fault zone (fault scarps, releasing basins, pressure ridges and offset streams) and disruptions of Pleistocene surfaces (Siame *et al.* 1997a, b; Fazzito *et al.*, 2013; Figure 2). The Pliocene-Quaternary activity of the El Tigre fault has been inferred by direct observation of the main and associated structures in trenches (Bastías *et al.*, 1984; Bastías, 1985; INPRES, 1982; Siame, 1998), by indirect observation along ERTs (Figure 2; Fazzito *et al.*, 2013), by paleomagnetic studies (Fazzito *et al.*, 2016), and by detailed slip-rates estimations (Siame *et al.*, 1997a, b). All this evidence suggested that the El Tigre fault was originated at Pliocene times (Fazzito *et al.*, 2016) and was reactivated and evolved during the Pleistocene (Fazzito *et al.*, 2013; Siame *et al.*, 1997a, b). Based upon geometrical variations along its strike, the El Tigre fault was divided into three major segments: the northern, central and southern segments

(Figure 2a; Siame *et al.* 1997b, Fazzito *et al.* 2013). In the northern segment, based on the analysis of seismic profiles and several outcrops, Álvarez-Marrón *et al.* (2006) interpreted a positive flower-type structure during the Neogene while Pérez and Costa (2011) observed transpressive deformation in outcrops of Neogene rocks with a dextral component. The southern segment of the El Tigre Fault (Figure 2a) is characterized by an almost pure dextral strike-slip component that offset alluvial surfaces labeled by Siame *et al.* (1997b) as A6 to A2 following a chronological order. Its recalculated exposures ages (Peri *et al.*, *under review*) by cosmogenic dating (^{10}Be) indicate an age span from 1,000 ± 100 ka to 135 ± 8 ka, respectively. Siame *et al.* (1997b) found that the tectonic activity of the El Tigre Fault has continued after 135 ± 8 ka (A2) with estimated horizontal and vertical slip-rates of 1 and 0.5 mm/a, respectively, since that time. In the central segment of the El Tigre Fault (30°47'07" - 30°49'08" S) (Figures 2a and b), its vertical component by dominant transtensive style disrupted the alluvial western piedmont of the Sierra del Tigre, configuring a scarp fault which exposes Neogene rocks (Rodeo Formation) and uplifted a western block (Figure 2). In this sector, the fault is expressed by an eroded east-facing scarp of 18 –24°dip (Bastías *et al.*, 1984) and a maximum height of ~85 m (Siame, 1998; Siame *et al.*, 1997a, b). Pressure ridges and releasing bends along the trace of the El Tigre fault (Fazzito *et al.*, 2013) indicate the presence of a strike-slip fault component (Figure 2), defining transpressional and transtensional sections, respectively. The western uplifted block preserves dissected alluvial fans, terraces and abandoned fluvial channels. The hanging wall is formed by dissected and undissected alluvial fans affected by the minor fault and fold scarps with Quaternary activity (Figures 2b). Previous ERT cross-sections suggest the presence of high angle east-dipping covered reverse faults (Fazzito *et al.*, 2013) related to some of these minor fault scarps. The alluvial fan terraces and the minor piedmont fault and fold scarps are the primary study object of this work in order to characterize its geometry and the relationship of these piedmont structures with the main structures as El Tigre fault and longitudinal thrusts of the Sierra del Tigre.

3. METHODOLOGY

3.1. GEOMORPHOLOGICAL AND STRUCTURAL MAPPING. TOPOGRAPHIC PROFILES

The present work comprised a detailed map of the geomorphology features of tectonic origin and Quaternary alluvial fan terraces located between the Sierra del Tigre to the east and the El Tigre fault to the west (Figure 2), based mainly on aerial and satellite images interpretation (Digital Globe-WorldView-4, 30 cm; Alos-Palsar Digital Elevation Model -DEM-, 12.5 m). The aggradation levels

were dissected and conformed alluvial fan terraces. In order to map and correlate the Quaternary alluvial fan terraces, which are well preserved under the present hyper-arid climate, we followed Siame *et al.* (1997a, b) and Terrizzano *et al.* (2014) criteria. These are based on deposit continuity, cut-and-fill relationships, relative topographic position, surface aspects such as desert pavement development and maturity, clast reddening (iron oxidation), clast burial and fracturing degree (Abrahams and Parsons, 1994; Christenson and Purcell, 1985; Hooke, 1967). We did not consider sedimentological characteristics as they are very similar in all units. The cosmogenic dating (^{10}Be) applied in the alluvial fan terraces yielded preliminary exposure ages (Peri *et al.*, 2018; *under review*) that broadly confirm those obtained for Siame *et al.* (1997a, b), which constitute an essential datum to corroborate and modify the preliminary mapping.

We identified in the study area several NNE-SSW trending fault and fold scarps affecting the Quaternary alluvial fan terraces on aerial and satellite data. In the field, we confirmed these structural scarps and anticlines by observation of flexures and disruptions of the terrace surfaces. The vertical displacement recorded by the scarps in the Quaternary alluvial fan terraces was measured along with several topographic profiles with Differential Global Positioning Systems (DGPS) in three selected locations in the northern, central and southern areas. The topographic survey was carried out with two DGPS, a Trimble 5700 and a Topcon HiPer SR with dual-frequency (L1, L2), with a precision of ± 1 m.

3.2. ELECTRICAL RESISTIVITY TOMOGRAPHIES: DATA ACQUISITION AND PROCESSING

The 2D electrical resistivity tomography (ERT) method was applied for modeling geological layers at subsurface and for characterizing Quaternary piedmont fault and fold scarps that affect the natural configuration of those Quaternary layers. A *Syscal R1 Plus Switch 48 Plus* Georesistivity-meter (*Iris Company*) was used to perform five surveys. The resistivity-meter can implement the entire sequence of measurement automatically by loading the information geometrical and acquisition parameters. The geometrical parameters delineate the array type, length of the potential and current dipoles and n level that is the rate between the separation of the current and potential dipole and the length of the current dipole. The geometrical array was performed with 48 electrodes spaced at 10 m (470 m full length), and extended to 72 electrodes (710 m full length) by the *roll-along* technique in one survey (Geoelectrical Profile B, Fazzito *et al.*, 2013) and 60 electrodes

in another one (Geoelectrical Profile A). The acquisition parameters define the maximum expected relative standard deviation of the resistivity measurement for each quadripole (quality factor), minimum and maximum numbers of stacks per measurement, current injection time per cycle and desired signal voltage. Values of the acquisition and geometric parameters are a conciliation between quality, duration of the survey and desired depth of investigation (Loke, 1996-2015). The quality factor is considered on the calculated values of apparent resistivity, which are obtained by the resistivity-meter immediately after the measurement of the voltage signal. Measurement parameters for the geoelectrical profiles are listed in Table 1.

Profile	Array type	Potential dipole length (m)	Depth level *n*	Section length (m)	Numbers of Quadripoles	Current pulse duration	Stack min-max	Expected standard deviation (%)	Maximum investigation depth of the 2D model (m)
A	DD (ra)	10 20	1-6 3,7/2, 4 9/2, 5, 11/2	590	87[illegible]	1	2-6	4	52
A	WS (ra)	10	1-18	[illegible]0	736	1	2-6	4	77
B	DD (ra)	10 20 30	1-6 3,7/2, 4 9/2, 5, 11/2, 6 4, 13/3, 1[illegible], 3[illegible] 5, [illegible]6/3, 17/3, [illegible] [illegible]9/3, 20/3, 7	710	1,322	1	2-4	3	60
C	DD	1[illegible]	1-6	470	639	1	2-6	4	55
D	DD	1[illegible]	1-6	470	639	1	2-6	4	52
D	WS	1[illegible]	1-18	470	504	1	2-6	4	77

Table 1. Geometrical and acquisition parameters used in each geoelectrical profile. It is also specified the maximum penetration depth of the numerical 2D resistivity model. The dipole–dipole array is indicated as DD, the Wenner–Schlumberger array as WS and ''ra'' points out the use of the roll-along method.

For every survey we choose the dipole-dipole array (Telford *et al.*, 1990) as it has been shown that provides very good imaging of high-angle faults (Caputo *et al.*, 2003, 2007; Collela *et al.*, 2004; Fazzito *et al.* 2009, 2013; Loke, 1996-2015; Ludwiniak *et al.*, 2019; Nivière *et al.,* 2008; Pánek *et al.,* 2011; Rizzo and Giampolo, 2019; Rizzo *et al.*, 2004; Terrizzano *et al.,* 2012) due to its high lateral sensitivity (Coggon, 1973). The Wenner-Schlumberger array provides a better image of horizontal

features such as geological layers due to its greater vertical sensibility. We applied this array in two profiles to compare with the dipole-dipole results. In the present study, the main objective of using this methodology has been to obtain information about the geometry of the possible geological structures related to the minor piedmont fold and fault scarps at the subsurface as well as on the geoelectrical layers at the subsurface in the western piedmont of the Sierra del Tigre and to define their relationship with main structures. We present the results of the pseudoresistivity measurements in the conventionally arranged form of pseudosections or pseudodepth plot (Telford *et al.*, 1990) of four ERTs carried out. These are contour color fill diagrams of pseudoresistivity values where the horizontal axis represents the geometrical midpoint of a quadrupole, and the vertical axis corresponds to the pseudodepth value (Figure 3). The four ERTs were distributed in three locations at the northern (Figures 4 and 5, Geoelectrical Profile A), central (Figures 6 and 7, Geoelectrical Profiles B and C) and southern (Figure 8, Geoelectrical Profile D) areas of the central segment of the El Tigre Fault, across minor fault and folds scarps. Among these ERTs we included in the central area, the Geoelectrical Profile B (Figures 6 and 7), which has been already published by Fazzito *et al.* (2013). The dipole-dipole array (Telford *et al.*, 1990) was applied in all profiles while the Wenner-Schlumberger array was applied in two profiles (Geoelectrical Profiles A and D; Figures 5 and 8). For this research, the resistivity modeling was solved numerically through the RES2DINV software (Loke 1996-2015; Loke and Barker 1996; Loke *et al.*, 2003). This model consists primarily of rectangular cells of constant resistivity that adjust the pseudoresistivity values measured at the surface up to an acceptable error. Typically, the dimension of the cells is related to the electrode spacing. The cell of the model discretization for the Geoelectrical Profile D -Dipole-Dipole array- (Figure 8c) and Geoelectrical Profile A -Dipole-Dipole array- (Figure 5a) has been set to the same width that the minimum electrode separation (10 m). For the rest of the presented models (Geoelectrical Profiles A, B, C and D -Wenner Schlumberger array-; Figures 5b, 7a, c and 8d) the cell was set to a width that is a half to the minimum electrode separation (5 m). The cell height for all models increases by 10% in each deeper layer (this option is chosen to admit the loss of resolution of the geophysical method with depth). About the non-uniqueness in the geophysical problem, both smoothness-constrained and robust inversion optimization methods (Loke *et al.*, 2003) were tried in data fitting in order to reduce the number of possible solutions. For the forward model subroutine, the finite-element method was applied. The topographic information was incorporated into the models by a uniformly distorted grid (all the grid nodes along the same vertical line are shifted the same distance according to the elevation of the ground surface). The results of the ERTs are described below. For the model

descriptions, the geoelectrical levels were defined based on resistivity values, lateral geometrical continuity, and resistivity contour configuration.

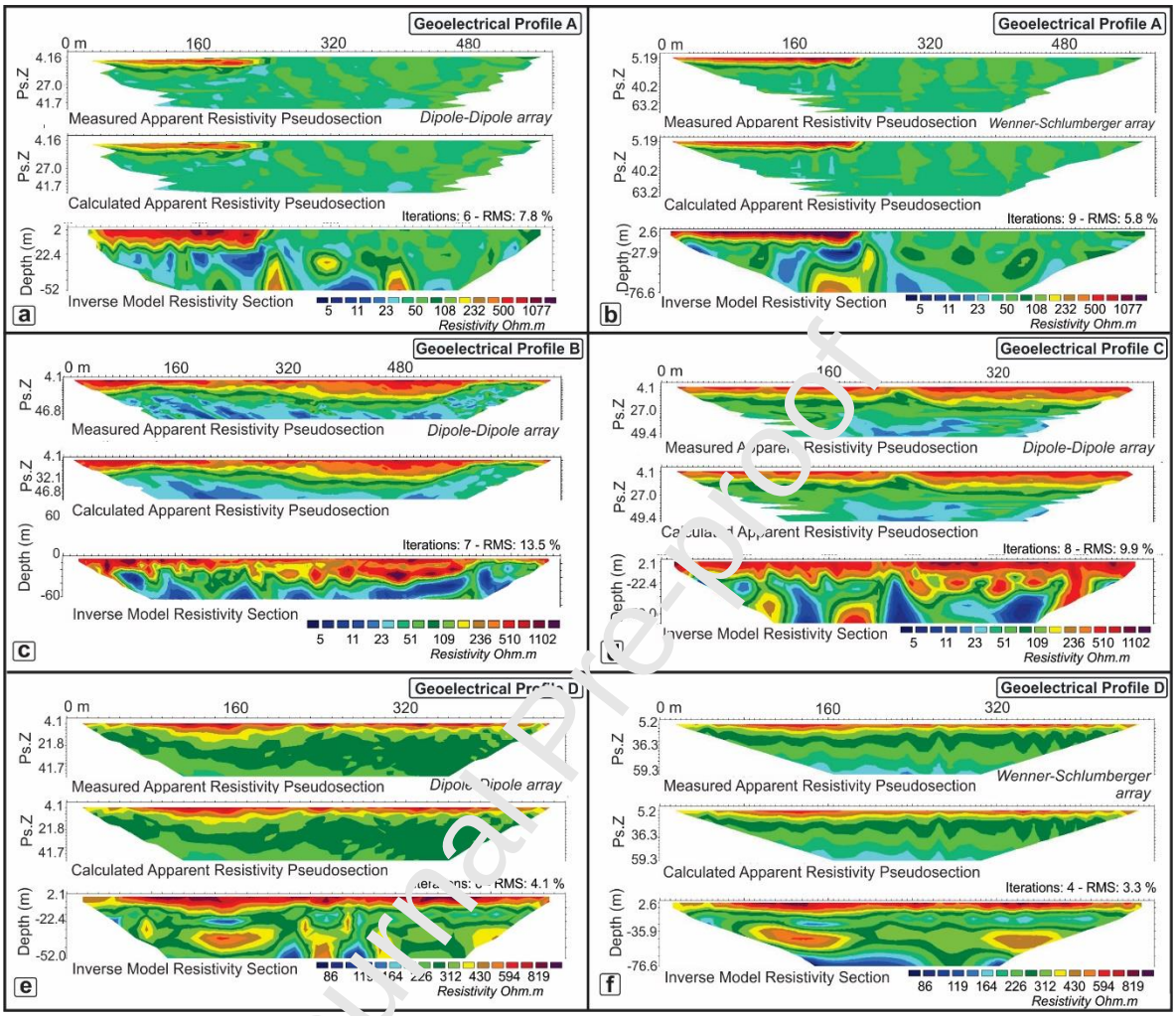

Figure 3. Measured and calculated Pseudosections. Pseudosections of measured and calculated apparent resistivity, and inverted models of Geoelectrical Profile A (a, b), Geoelectrical Profile B (c), Geoelectrical Profile C (d), and Geoelectrical Profile D (e, f). **3-COLUMNS**

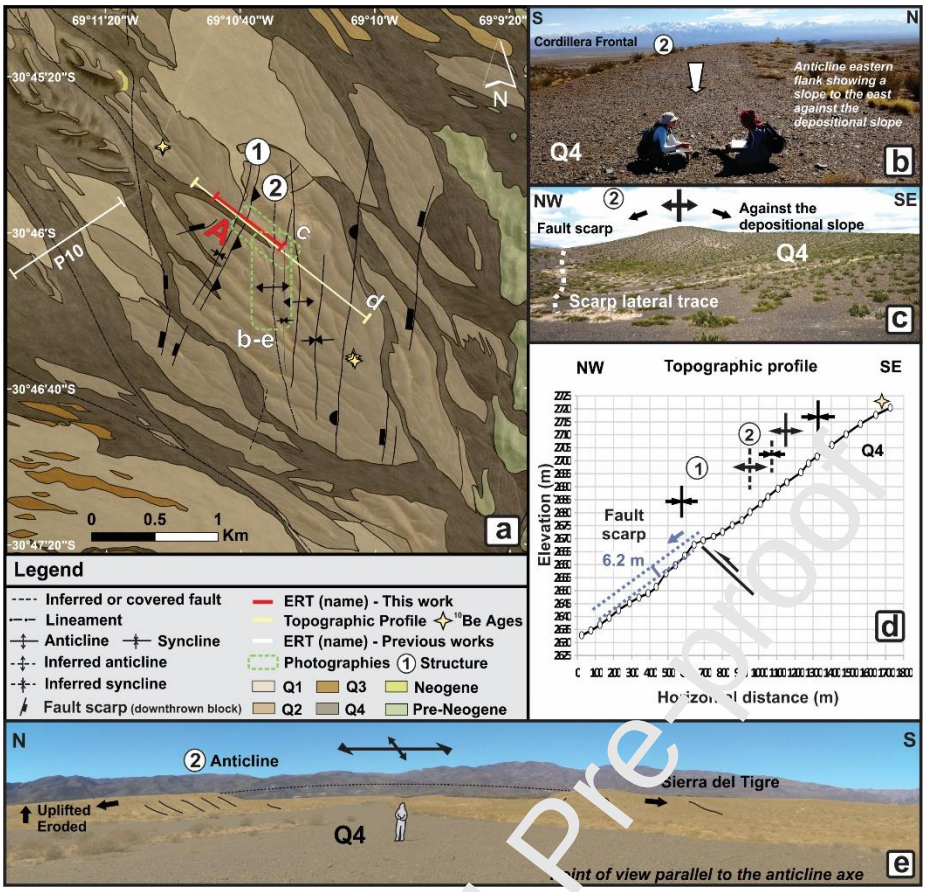

Figure 4. Northern area. a) Geological map of the northern area. The trace of topographic and geoelectrical profiles and piedmont scarps photographs are indicated. White lowercase letters indicate the localization of figures. The main studied structures are numbered. b) View to the northeast of the antidine (2). c) View to the west of the E-dipping flank of the anticline (2) developed on the alluvial fan terrace Q4. Tilt against the depositional slope of the alluvial fan terrace Q4, and the lateral trace of the fault scarp associated to the anticline are shown. d) Topographic profile across the main piedmont morphotectonic features. A vertical offset of the west-facing fault scarp (1) was estimated. e) View to the east of the anticline (2). Erosion is visible at the center of the antidine. **2-COLUMNS**

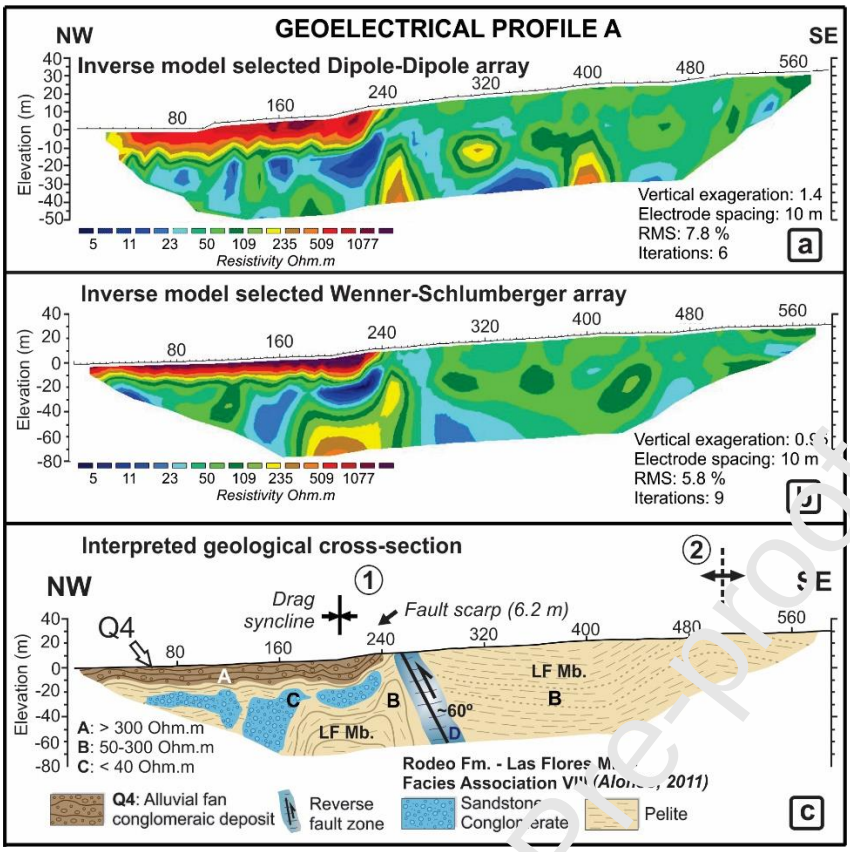

Figure 5. Northern area. a) Geoelectrical Profile A (localization in Figure 4a). The selected inverse model performed from a dipole-dipole array with a unit electrode spacing of 10 m. The maximum penetration depth was 52 m. b) The selected inverse model performed from Wenner-Schlumberger array with a unit electrode spacing of 10 m. The maximum penetration depth was 77 m. c) Interpreted geological cross-section. **2-COLUMNS**

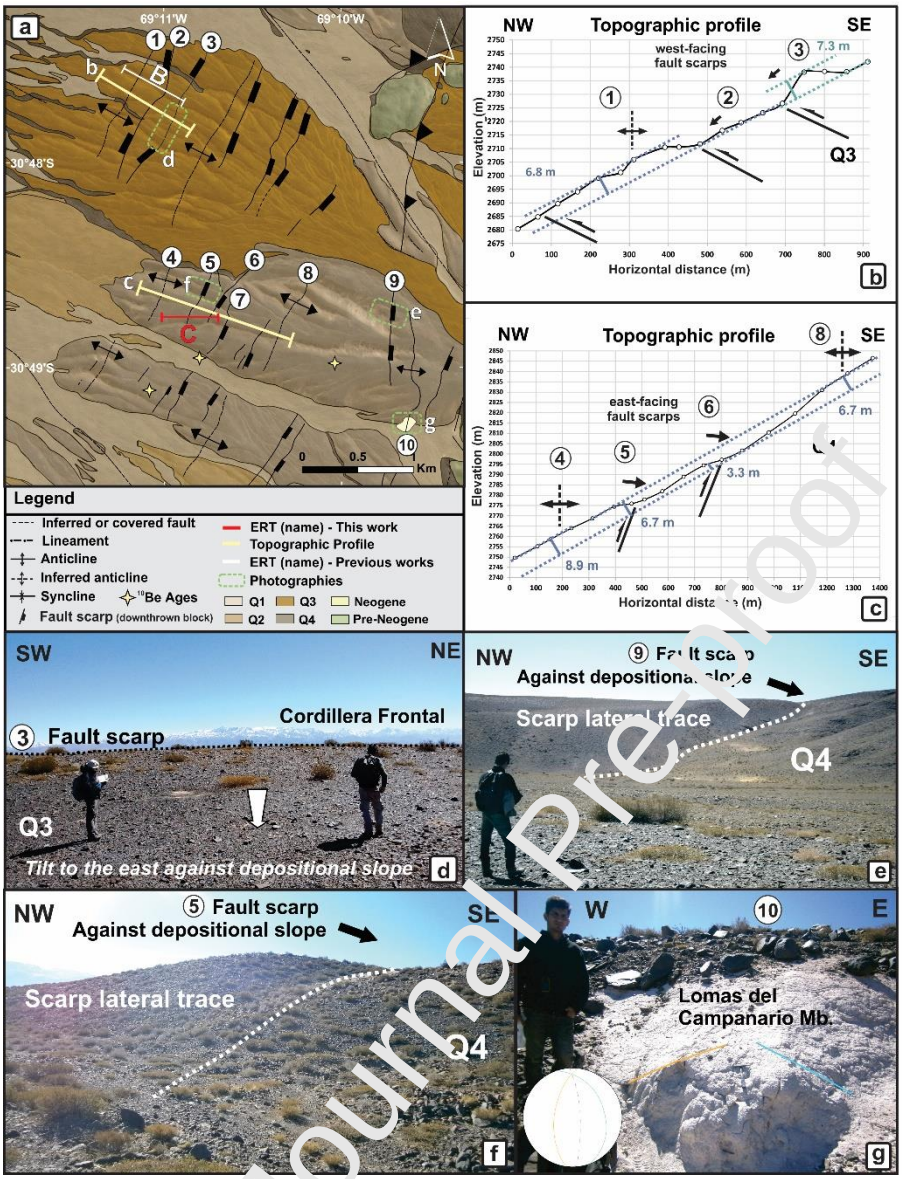

Figure 6. Central area. a) Geological map of the central area. The trace of topographic and geoelectrical profiles and piedmont scarps photographs are indicated. The main studied structures are numbered. White lowercase letters indicate the localization of figures. b) Topographic profile across some of the main piedmont morphotectonic features of the alluvial fan terrace Q3. Vertical offsets of an anticline (1) and a west-facing fault scarp (3) were estimated. c) Topographic profile across some of the main piedmont morphotectonic features of the alluvial fan terrace Q4. Vertical offsets of anticlines (4, 8) and east-facing fault scarps (5, 6) were estimated. d) View to the northwest of the fault scarp (3) developed on the alluvial fan terrace Q3. e, f) View to the northeast of east-facing fault scarps (9, 5) developed on the alluvial fan terrace Q4. Tilt towards the east of the alluvial terrace Q4 against the depositional slope, and the lateral traces of the fault scarps are shown. g) View to the north of an anticline (10) developed on Lomas del Campanario Member (modified from Pérez, 2018). **2-COLUMNS**

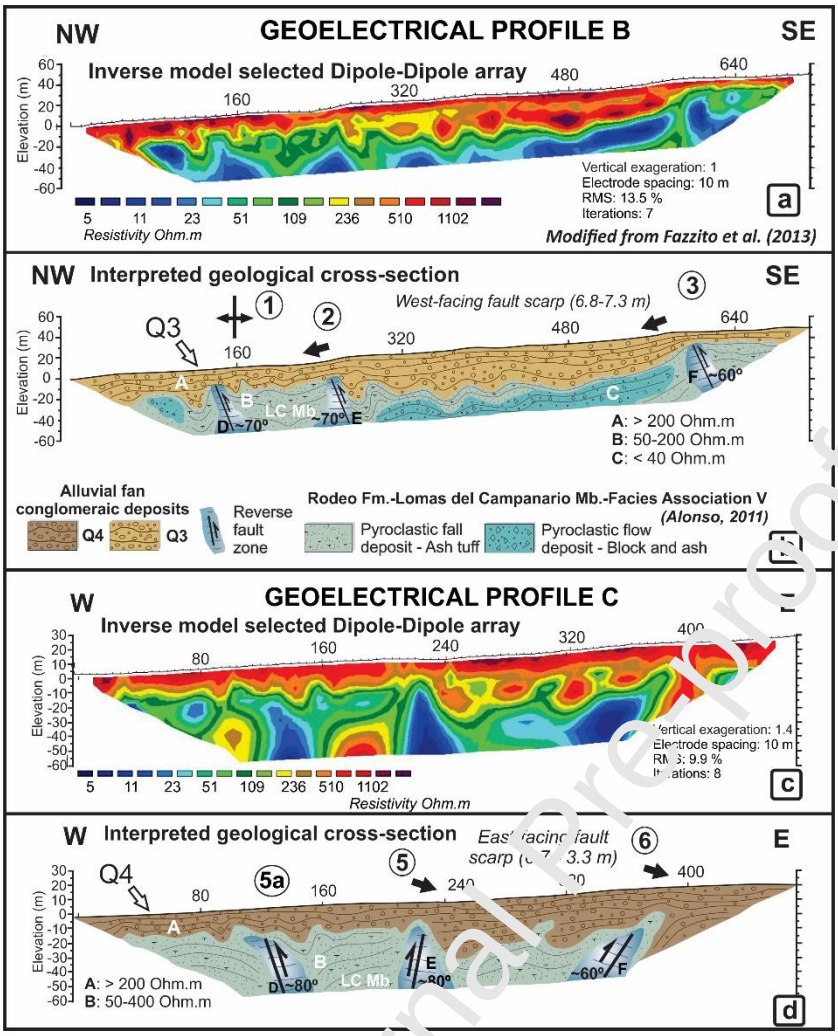

Figure 7. Central area. a) Geoelectrical Profile B (localization in Figure 6a). The selected inverse model performed from a dipole-dipole array with a unit electrode spacing of 10 m. The maximum penetration depth was 60 m. b) Interpreted geological cross-section of (a). c) Geoelectrical Profile C. The selected inverse model performed from a dipole-dipole array with a unit electrode spacing of 10 m. The maximum penetration depth was 55 m. d) Interpreted geological cross-section of (c). **2-COLUMNS**

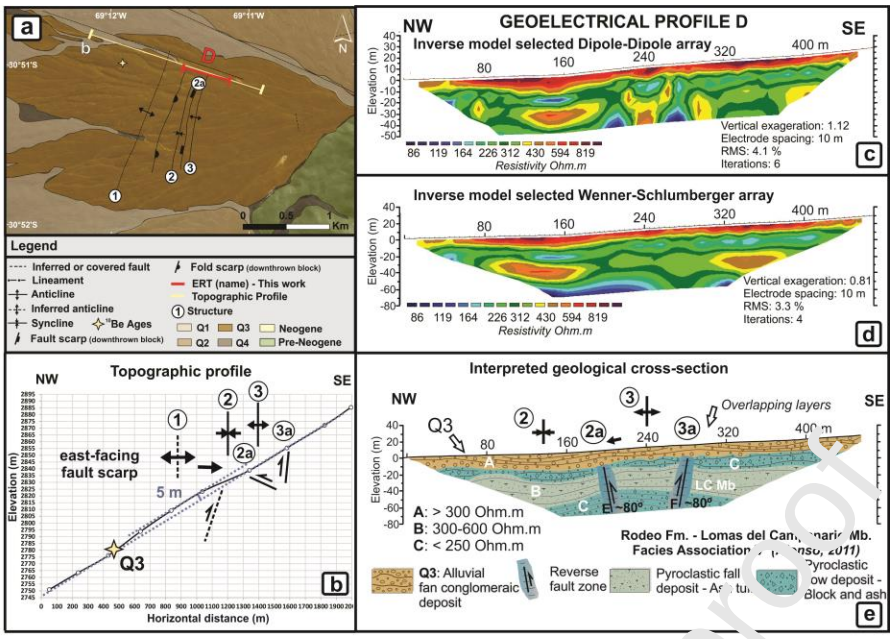

Figure 8. Southern area. a) Geological map of the southern area. The trace of topographic and geoelectrical profiles are indicated. The main studied structures are numbered. White lowercase letters indicate the localization of figures. b) Topographic profile across the main piedmont morphotectonic features. A vertical offset of the east-facing fold scarp (1) was estimated. c) Geoelectrical Profile D. The selected inverse model, performed from a dipole-dipole array with a unit electrode spacing of 10 m. The maximum penetration depth was 52 m. d) The inverse model chosen performed from Wenner-Schlumberger array with a unit electrode spacing of 10 m. The maximum penetration depth was 77 m. e) Interpreted geological cross-section. **2-COLUMNS**

4. RESULTS

4.1. GEOMORPHOLOGICAL AND STRUCTURAL MAPPING. TOPOGRAPHIC PROFILES

The western piedmont of the Sierra del Tigre is a broad *bajada* integrated by different generations of Quaternary alluvial fans. The alluvial deposits unconformably cover the pre-Quaternary basement. Provenance is from the Sierra del Tigre in the East and they are formed mainly by volcanic and metamorphic clasts of its Ordovician basement (Yerba Loca Formation). The El Tigre Fault scarp disrupted piedmont with an N-S direction and configured a western uplifted block in which wind and water gaps on alluvial deposits were preserved (Figure 2). The Quaternary mapping was focussed in the eastern hanging wall of the El Tigre fault, where the identification of the different alluvial fan deposits was feasible (Figure 2b). The relative stratigraphic relationship and fan surface morphology of the alluvial fan units were consistent with those previously described for the southern segment of the El Tigre Fault (Siame *et al.*, 1997a, b; Figure 2a). At the surface, the

oldest alluvial fans show the same dissection grade and well-developed desert pavement, which indicates past semi-arid conditions (Staley *et al.*, 1991), deflation and periglacial processes during long abandonment periods of the alluvial system.

On the other hand, local vertical motion on the central segment along the El Tigre Fault increased the entrenchment of alluvial fan units in comparison to the southern segment. Along the east-facing steepened scarp of the El Tigre Fault (Figure 2), these alluvial fan terraces were beheaded and deformed in restraining and releasing stepovers due to the fault activity (Figure 2b). The minor east- and west-facing fault and fold scarps have been developed on the alluvial fans (Figure 2b), modifying the original design of the drainage network. We identified four Quaternary alluvial fan terraces (Q4, Q3, Q2, Q1) and the current fluvial-alluvial unit (Q0), channeled between the oldest ones. The oldest alluvial fan terraces were called Q4 and Q3 and the deposits associated are conglomerates composed by fine subrounded to subangle clasts, matrix- and clast-supported, with moderately to poorly consolidation. They are composed of 1-3 cm size clasts of volcanites (andesites and basalts) and metapsamites of the Ordovician basement exposed in Sierra del Tigre. These units show a well-developed desert pavement with dark greyish to blue-greyish color (Figures 4b, c, e, and 6d-g), and a half thickness clasts buried. Clast reddening and a moderate clast fracturing degree were observed. The alluvial fan terrace Q4 is relatively more elevated than Q3 and was preserved as relics because after its deposition was exposed to lateral erosion, decreasing its areal distribution, being at present highly dismembered. The youngest alluvial fan terraces were called Q2 and Q1, and the deposits associated are fine conglomerates with similar sedimentological characteristics to the oldest units. Q2 and Q1 have, however, smaller clasts, a more whitening matrix, and a lower degree of consolidation than of the oldest deposits. In some areas, they are unconsolidated. Some clasts seem reworked from alluvial fan terrace Q3 and show reddening at the surface. The alluvial fan terrace surface shows poor development of desert pavement, very shallow clasts buried, and minor clast reddening. Low clast fracturing was observed. Unit Q2 appears at lower altitudes than Q3. The deposit Q1 lies between the oldest alluvial fan terraces (Q4, Q3, and Q2) and shows subtle bars as evidence of depositional features. Finally, Q0 is the current fluvial and alluvial deposit, very similar to alluvial fan terrace Q1. Unit Q0 consists of an unconsolidated material with very rounded clasts. This deposit has neither desert pavement nor clasts buried, clast reddening, or fractures, and it lies in the current ephemeral streams between the oldest alluvial fan terraces.

Both main and minor faults and folds with recent activity partially affect the Quaternary landscape evolution in the study area. As it was mentioned before, the El Tigre Fault generated the main fault scarp that disrupted piedmont and the alluvial fan terraces and configured a western uplifted block and an eastern hanging wall. Meanwhile, minor scarps segmented the alluvial fan terraces (Figures 2b, 4a-c, e, 6a-f), affecting their natural topographic profiles and provoking confine vertical erosion in the elevated blocks. To accurately quantify the vertical displacements of the alluvial fan terraces, the study area was analyzed with topographic profiles from DGPS data at a local scale (Figures 4d, 6b, c, and 8b), in three selected sites at northern (Figure 4), central (Figure 6), and southern (Figure 8) locations. In the northern area, one profile across a west-facing fault scarp and several fold scarps on the oldest alluvial fan terrace Q4 produced displacements of 6.2 m ± 1 m (Figure 4d). In the central area, two profiles were surveyed across several east-facing fault scarps and several inferred anticlines. The northern alluvial fan terrace of this area interpreted as Q3 shows at its distal part (Figures 6b), near to the El Tigre Fault, vertical displacements of 6.8 and 7.3 m. The southern alluvial fan terrace of this area Q4 shows displacements of 8.9 and 6.7 m (Figures 6c), and from these values, we inferred a mean vertical offset of 7.8 m ± 1 m. A minor fault scarp produced a displacement of 3.3 m (Figures 6c), but we did not consider this anomalous value in the vertical offset average. In the southern area, one profile across an east-facing fault scarp and several fold scarps on the alluvial fan terrace Q3 produced displacements of 5 m ± 1 m (Figure 8b).

4.2. 2D GEOELECTRICAL DESCRIPTION AND GEOLOGICAL INTERPRETATION

Geoelectrical Profile A

Description: Apparent resistivity values with standard deviation over 25 % were discarded, and the consequent percentage of data used for resistivity modeling was 98 % of the recorded data at the field for both arrays. The misfit between the calculated values of apparent resistivity and those recorded in the field data is expressed through the root mean square (RMS) which was 7.8 %, after six iterations, for the dipole-dipole array and 5.8 %, after nine iterations for the Wenner-Schlumberger array. The maximum depth of the model for the dipole-dipole and Wenner-Schlumberger arrays, were 52 and 77 m, respectively. For this electrical survey, it has been observed that the calculated pseudosections were similar to the pseudosections corresponding to the field measurements and differed only in minor features (Figures 3a and b). The description and interpretation were made by integrating both 2D ERT model inversions taking into account that

dipole-dipole array shows better the vertical features such as faults, while the Wenner-Schlumberger array has a better horizontal resolution remarking geoelectrical levels. Three geoelectrical levels were identified (Figure 5). The level called A was observed at the NW extreme and showed the higher resistivity values (> 300 Ohm.m) of the model that continued into the subsurface at depths around 15 m. Level A had a subhorizontal configuration that turned to a curved plane toward the profile center between 200 and 240 m, changing its horizontal disposition to a gently NW-dipping. The level called B was observed at the SE zone of the profile and showed intermediate resistivity values (between 50 and 300 Ohm.m), reaching from the surface into the subsurface until the bottom of the model at depths around 60 m. Level B had a curved plane configuration in the SE zone of the profile, turning into a very irregular one in the NW zone. Internally, this zone shows a conspicuous high-angle (~60°), SE dipping, low resistivity discontinuity (15-40 Ohm.m) called D (between 250 and 280 m) that denote the sharp lateral change on geometry configuration of level B as well as the absence of level A at the SE zone of the profile. In the NW zone, a level called C was identified with the lowest resistivity values (< 40 Ohm.m), which is intercalated in the level B. Level C is observed between 20 and 40 m deep and shows lateral interruptions.

Interpretation: Level A coincides in surface with the alluvial fan terrace Q4 exposed in the NW zone of the profile (Figures 4b, c, e and 5c). The horizontal geometry of this level can be interpreted as a horizontal stratification, which turned to NW-dipping toward the center of the profile (200-240 m), in which curved shape could represent a drag syncline (Figure 5c; structure 1). Level B represents the substratum rocks under the Quaternary sediments (Figure 5c). According to the lithologies described in the Facies Association VIII of the Las Flores Member, Rodeo Formation, that has been reported by Alonso (2011) in this area of piedmont, and the surrounding outcrops described by Pérez (2018), the substratum rocks of Level B can be assigned to pelites (Figure 5c) of this facies association. Level B shows an irregular configuration in the NW zone, plus the presence of an intercalated conductive layer called level C (Figure 5c). According to the lithologies described for the same Facies Association VIII of the Las Flores Member (Alonso, 2011), Rodeo Formation, and the surrounding outcrops (Pérez, 2018), Level C can be interpreted as a sandstone-conglomerate lithology, that functions as an aquifer. Finally, the discontinuity evidenced by the high-angle conductive zone called D can be interpreted as a ~60° SE-dipping reverse fault of west vergence (Figure 5c; structure 1) that uplifted the Neogene rocks in the southeastern block. The preliminary west-facing fault scarp mapped (Figures 4a, d, and 5c) coincides with the subsurface fault zone

observed in this model. The absence of the alluvial fan terrace Q4 in the uplifted block is consistent with the local erosion seen at the surface (Figures 4e and 5c). The syncline affecting the alluvial fan terrace Q4 can be interpreted as a consequence of the displacement of the reverse fault.

Geoelectrical Profile B

Description: This model was already published by Fazzito *et al.* (2013). Apparent resistivity values with standard deviation over 4 % were ruled out, and the following percentage of data used for resistivity modeling was 93 % of the total recorded. The RMS for the dipole-dipole array was 13.5%, after seven iterations. The maximum depth of the model for the dipole-dipole was 60 m. The calculated pseudosection were roughly similar to the pseudosection corresponding to the field measurements and differed only in minor features (Figure 3c). Three geoelectrical levels were identified (Figures 7a and b). The level called A showed the higher resistivity values (> 200 Ohm.m) of the model and is extended through the whole profile from the surface to a depth of 10 to 20 m, increasing to approximately 40 m between 260 and 570 m (Figures 7a and b). Level A shows a subhorizontal configuration with some NW-dipping in the thickest zone (Figures 7a and b). The level called B shows intermediate resistivity values (50-200 Ohm.m) and extends along with the whole profile at depths of 20 to 40 m below the surface until the bottom of the model. Level B has an intercalated layer called level C that shows the lowest resistivity values (< 40 Ohm.m), appearing between 260 and 570 m, at variable depths of 20 to 40 m below the surface down to the bottom of the cross-section (Figures 7a and b). Level C shows an apparent discontinuous character and a reduced extension at the northwestern zone of the profile (Figures 7a and b). Three high-angle (~60°-70°) SE-dipping zones of low resistivity values (10-40 Ohm.m) were identified and called D, E, and F (Figures 7a and b).

Interpretation: Level A coincides in surface with the alluvial fan terrace Q3 (Figures 6a and 7b). The horizontal geometry can be interpreted as a horizontal stratification, which between 260 and 570 m is thicker and shows an NW-dipping (Figure 7b). This thickest zone is bounded at the surface by two west-facing fault scarps (Figures 6a, b, and 7b; structures 2 and 3). Level B is interpreted as the rock substratum under the Quaternary sediments (Figure 7b) until the bottom of the profile. According to the lithologies described in the Facies Association V of the Lomas del Campanario Member, Rodeo Formation, that have been reported by Alonso (2011) in this area of piedmont, and to the near outcrops described by Pérez (2018), the substratum rocks of Level B can

be assigned to ash tuffs (Figure 6g and 7b) of this facies association. The conductive level C can be assigned to a block and ash lithology that belongs to the same Facies Association V (Alonso, 2011), a more porous rock that may be working as an aquifer (Figure 7b). The conductive zones called D, E, and F were interpreted as approximately ~60° to 70° SE-dipping reverse faults of west vergence (Figure 7b; structures 1, 2, and 3) that displaced or uplifted the Neogene rocks. The preliminary west-facing fault scarps mapped (Figures 6a, b, and 7b) coincide with the subsurface fault zones observed in this model. The two high angle east-dipping faults E and F that limit the thickened Q3 coincide with the topographic scarps (Figure 6a, b, and 7b). However, it must be considered that the features used to identify the presence of faults in previous models (sharp resistivity contrasts, narrow subvertical conductive zones, etc.) are more ambiguous in this model.

Geoelectrical Profile C

Description: This profile was surveyed at less than 2 km south of Geoelectrical Profile B (Figure 6a). Apparent resistivity values with standard deviation over 25 % were ruled out, with 97% of the recorded initially data left to be used for resistivity modeling. The RMS for the dipole-dipole array was 9.9%, after eight iterations. The maximum depth of the model for the dipole-dipole was 55 m. Both calculated and measured pseudosections were roughly similar (Figure 3d). In general, the tomographic model is very similar to that of geoelectrical profile B (Figures 7a and c). Two geoelectrical levels were identified (Figures 7c and d). The level called A shows the higher resistivity values (> 200 Ohm.m) and extends along with the whole profile from the surface down to a depth of 20 m, which is increased to approximately 40 m between 230 and 380 m (Figures 7c and d). Level A shows a subhorizontal configuration with a gently W-dipping attitude in the thickest zone and a more complex character in the western zone of the cross-section (Figures 7c and d). Level B shows intermediate resistivity values (50-400 Ohm.m) and is extended through the whole profile at depths of 20 to 40 m below the surface down to the bottom of the model. Level B shows significant heterogeneity due to the presence of three high-angle (~60°-80°) dipping zones of low resistivity values (< 30 Ohm.m), one E-dipping (Figure 7d; structure 5a) and two W-dipping (Figure 7d; structures 5 and 6) called D, E, and F, respectively.

Interpretation: Level A (Figure 7d) corresponds in the surface (Figure 6a) with the oldest alluvial fan terrace Q4. Its geometry and attitude suggest a horizontal stratification becomes thicker and gently W-dipping between 230 and 380 m (Figure 7d). This thickest zone is bounded at the

surface by two east-facing fault scarps (Figures 6a and c, and 7d; structures 5 and 6). Level B is interpreted as representing the substratum rocks under the Quaternary sediments (Figure 7d) down to the bottom of the whole profile. As well as in the geoelectrical profile B, level B can be correlated to ash tuff lithology of the Facies Association V (Alonso, 2011) of the Lomas del Campanario Member (Rodeo Formation) due to the presence of outcrops of this lithology in the head of the same alluvial fan terrace (Pérez, 2018; Figures 6a and g). Internally, level B shows an irregular configuration mostly due to the conductive zones (D, E and F) approximately ~60°-80° E- and W-dipping interpreted as reverse faults of west and east vergence (Figure 7d; structures 5a, 5, and 6) that interrupted, displaced and uplifted the Neogene rocks. The east-facing fault scarps mapped (Figures 6a and c, and 7d; structures 5 and 6) coincide with the subsurface fault zones observed in this model. The two high angle west-dipping faults E and F are the boundaries of the thickened Q4, in coincidence with the topographic scarps (Figure 6a and c, and 7d). On the other hand, the conductive zone D interpreted as a reverse fault of west vergence (Figure 7d; structure 5a) cannot be related to any feature observed at the surface.

Geoelectrical Profile D

Description: Apparent resistivity values in this survey show standard deviation values under 25 % consequent 100 % of recorded data was used for resistivity modeling with both arrays. The RMS was 4.1 % for the dipole-dipole array, after six iterations, and 3.3 % for the Wenner-Schlumberger array, after four iterations. The maximum depth of the model for the dipole-dipole and Wenner-Schlumberger arrays, were 52 and 77 m, respectively. Both calculated and measured pseudosections were roughly similar (Figures 3e and f). The description and interpretation were made by integrating both 2D model inversions. All geoelectrical levels identified in the geoelectrical profile D show an excellent horizontal resolution in the Wenner-Schlumberger model (Figure 8d), while two subvertical highly conductive features are better defined in the dipole-dipole model (Figure 8c). Three geoelectrical levels were identified (Figures 8d and e). Level A was observed across the whole profile with the highest resistivity values (>300 Ohm.m) of the model and extends from the surface down to depths around 10 to 20 m (Figure 8e). It shows a subhorizontal configuration that turned to a curved plane toward the northwestern sector of the profile between 80 and 180 m. To the center of the profile, this level inverts its curved shape, mainly between 190 and 310 m. Level B also is observed across the whole profile with similar resistivity values to level A but restricted

between 300 and 600 Ohm.m, and is developed between 20-30 and 40-60 m deep, following the same geometry configuration that A (Figure 8e). However, this layer is interrupted in two zones between 180 and 200 m, and 270 and 290 m (Figures 8c and e). Level C shows higher conductivity values (< 250 Ohm.m) and is observed as two different layers (Figures 8c and e). The upper one has a similar geometric configuration that level A, which is a down curved plane at the northwestern zone of the profile inverted at the central zone. Notably, this upper layer C shows the same horizontal interruptions (Figures 8d and e). The lower layer C is developed below level B, at depths between 40 and 60 m down to the bottom of the profile. Two high-angle (~80°), SE- and NW-dipping, low resistivity (< 200 Ohm.m) discontinuities between 180 and 200 m (E) and between 270 and 290 m (F), respectively, produce the sharp lateral interruption on level B and upper layer C.

Interpretation: Level A coincides in surface with the alluvial fan terrace Q3 exposed along with the complete profile (Figures 8a and b). The horizontal attitude of this level can be interpreted as a horizontal stratification which turned into an open syncline at the northwestern zone, and an open anticline at the central area of the cross-section (Figure 8e; structures 2 and 3). Moreover, the geometry of the level A suggests that it represents an overlapping layer (Figure 8e). Levels B and C represent the substratum rocks under the Quaternary sediments (Figure 8e). The geological context and surrounding outcrops allow interpreting that this substratum rocks correspond to the Facies Association V (Alonso, 2011) of Loma del Campanario Member (Rodeo Formation). Level B can be interpreted as ash tuff lithology while the more conductive level C as block and ash lithology with higher porosity. Levels B and C follow the same geometric configuration that level A, by describing an open synclinal to the northwestern zone of the profile, and an anticline at the center (240 m). The two conductive zones (E, F) are interpreted, respectively, as SE- and NW-dipping reverse faults (Figure 8e; structures 2a and 3a) that uplifted the Neogene rocks and folded the Quaternary deposit. The preliminary west-facing fault scarp mapped (Figure 8a; structure 2a) coincides with the SE-dipping fault observed in this model (Figure 8e; structure 2a). No significant displacements of the geoelectrical levels are evident at the fault zones.

5. DISCUSSION

Geological units, structural style and tectonic regime

Electrical resistivity models indicate that the Quaternary alluvial fan terrace deposits Q3 and Q4 are characterized by high resistivity values (> 200-300 Ohm.m) and horizontal stratification, with

local folded shapes as well as variable thickness associated to the presence of fault structures. The deepest electrical levels represent the substratum rocks with intermediate resistivity values (50 to 300-600 Ohm.m) and also show some low-resistivity intercalated layers or zones (< 30-40 Ohm.m; < 250 Ohm.m at the south). In agreement with the geological context and surroundings outcrops, at the northern area (Figures 4 and 5), these substratum rocks are correlated to the Facies Association VIII of Las Flores Member, Rodeo Formation (Alonso, 2011), characterized by pelites (intermediate resistivities) and sandstones-conglomerates (highest conductive layers). On the other hand, at the central and southern areas, substratum rocks are correlated to the Facies Association V of Lomas del Campanario Member, Rodeo Formation (Alonso, 2011). The more resistive layers are interpreted to be represented by ash tuff while the more conductive interlayers may represent block and ash deposits. Outcrops of gently folded ash tuff at proximal zones of the alluvial fan terrace deposits Q4 in the central area (Figure 6g) confirm the presence of Lomas del Campanario Member under the Quaternary deposits. The most conductive levels at north and south are likely more porous rocks that probably work as aquifers. The water table in the surveyed area is most likely located between 20 and 40 m deep, which is in agreement with the results obtained by Fazzito *et al.* (2013). It is worth pointing out that the systematic disturbance that subvertical conductive zones provoke in the aquifers suggests that faults may be acting as hydrogeological barriers in this region (see also Fazzito *et al.*, 2013).

ERTs models allow us to identify fault zones characterized by a) lateral discontinuity of resistivity values, b) abrupt changes in the geometric configuration at both sides of structures, c) highly conductive (< 50 Ohm.m) subvertical zones, features that are commonly observed at faults (Fazzito *et al.*, 2009, 2013; Petrit *et al.*, 2018; Targa *et al.*, 2019; Terrizano *et al.*, 2012). The highly conductive values are interpreted as being the product of the presence of fragmented, disintegrated, unconsolidated and, therefore more porous rocks as a consequence of the rupture associated to the displacement along the plane fault and the water percolation, ascent and/or lateral circulation inside the rock mass. These processes tend to decrease the resistivity values of the fault zone. All faults identified here are interpreted as reverse faults due to the following evidence:

i) In the northern area (Figure 5c), the eastern block seems to have been uplifted and the absence of the alluvial fan terrace Q4 at its surface strongly suggests the erosion of those deposits, in

agreement with the surface erosion observed; while the western block shows a drag syncline affecting the Q4 deposit.

ii) In the central area (Figures 7b and d), the alluvial fan terraces Q3 and Q4 show significantly thicker zones, bounded by high angle fault zones that have tilted these deposits. The geometrical configuration observed between east- and west-facing fault scarps and W- and E-dipping faults, respectively, suggests the presence of reverse faults in all the cases. It is worth to mention that in the proximal part of these alluvial fan terraces, the presence folded layers of ash tuff of the Lomas de Campanario Member under the Quaternary deposits (Figures 6a and g; structure 10) show clear evidence that the deformation also affects the substratum.

iii) In the southern area (Figure 8e), an open anticline and syncline are associated with a covered and conjugate fault set which disrupts, uplifts and folds the Neogene substratum and the alluvial fan terrace Q3.

Following the above-described observations, the piedmont deformation studied here is divided into two groups of structures. The main group is constituted by E-dipping and west vergence reverse faults associated with gentle asymmetric anticlines and drag synclines. This group is located at the distal zone of alluvial fans, near to the El Tigre Fault (Figure 9; frontal splay and main anticline). The subordinated group is constituted by antithetic W-dipping and east vergence reverse faults associated with gentle anticlines. This group is located in the central and proximal zones of the alluvial fans, near to the Sierra del Tigre (Figure 9). Additionally, the magnitude of the tectonic deformation seems to increase to the north. In the south, the frontal anticline associated to the main group of structures, it is slightly expressed at the surface with the lowest topographic scarp displacement (Figure 8b, 5m), and it shows an inner arc tighter than the outer arch that configures overlapping Quaternary (Q3) layers (Figure 8e). This geometrical configuration in the south evidence that the uplift rate is lower than the depositional rate. On the other hand, in the central and north locations, the frontal west vergence fault and main anticline evidence the highest topographic scarp displacements (Figures 4d, 6b and c; ~6-9 m) and a notorious erosion in the uplifted block (Figure 5c), a process that can be related to a higher uplift than in the south. In conclusion, the structural model is characterized by a frontal west vergence thrust fault associated with a main anticline and minors synclines, which are better expressed at the surface toward the north, and by several subordinated backthrusts of east vergence associated with minors anticlines. The entire

deformation belt clearly corroborates a section dominated by a compressive component of strain, where the backthrusts also relieve the tectonic deformation in this piedmont.

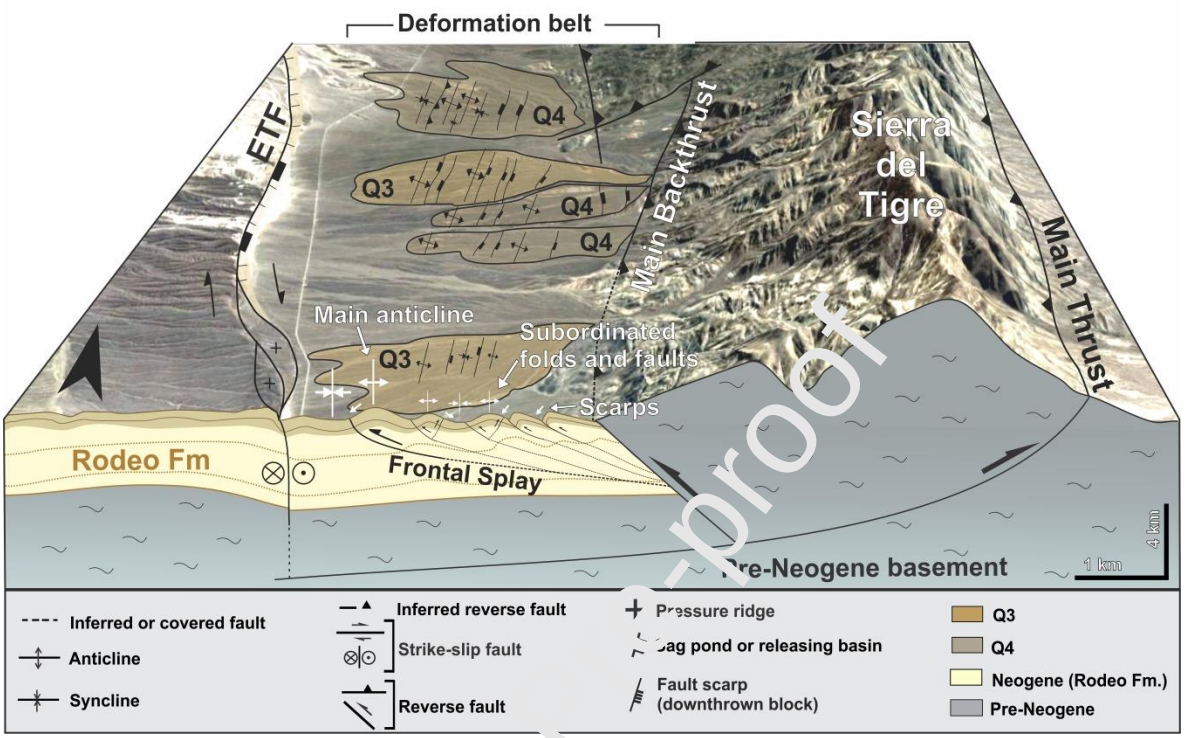

Figure 9. 3D structural model interpretation. ETF: El Tigre fault. **3-COLUMNS**

Relation to main structures and timing of deformation

The structural style of the minor piedmont deformation revealed here is probably related to the main structures and the tectonic events registered in the study area. The Sierra del Tigre, as part of the Western Precordillera, was uplifted under a transpressive regime during the last ~15-13 Ma (Allmendinger and Judge, 2014; Levina *et al.*, 2014; Suriano *et al.*, 2017; Walcek and Hoke, 2012) by an east vergence main thrust (Figures 1b, c, and 9), which is the main structure still poorly studied. Probably coeval to the main uplift, an antithetic backthrust of this range (Figures 1c, 2 and 9) was developed to accommodate the tectonic deformation. On the other hand, the main piedmont structure, the El Tigre Fault, represents a dextral strike-slip fault with vertical component determined by observations in trenches (Bastías *et al.* 1984, Bastías 1985; INPRES, 1982; Siame 1998), and ERTs (Fazzito *et al.*, 2013). This fault has been active since the Pliocene (Fazzito *et al.*, 2016) until Holocene times (Siame *et al.*, 1997 a, b), as established from paleomagnetic studies and cosmogenic dating, respectively. Other regional structures affecting the study region are ~NW-SE

lineaments (Figure 2) that obliquely intersect the El Tigre Fault without evident offsets, and are related to subvertical faults with a possible sinistral strike-slip kinematics as determined from ERTs (Peri *et al.*, 2017). These lineaments can be constrained to the Pliocene-Early Pleistocene because it mainly affects the Neogene Rodeo Formation. These structures are probably linked to old transversal Precordilleran structures (Peri *et al.*, 2017), reactivated at central segment of the El Tigre Fault (Figures 2). During the Quaternary evolution of the El Tigre Fault, reactivation of these lineaments controlled the strain distribution both in the main fault as well as in the minor faults and folds studied here (Peri *et al.*, 2017). During Holocene times, both the El Tigre Fault scarp and the minor piedmont scarps underwent tectonic activity as evidenced by the modified current drainage network and morphometric parameters (Peri *et al.*, 2018; *under review*).

In our study area, the El Tigre Fault is characterized by a dominant transtensive style, which contrasts with the compressive structures interpreted in the ERTs of the Sierra del Tigre piedmont. Thus, the results obtained and the structural style interpreted here suggest that the main piedmont thrust (Figure 9) constitutes a frontal splay of the western vergence backthrust of the Sierra del Tigre. Therefore, the piedmont deformation belt is better explained by a connection to the compressive component that uplifts the Sierra del Tigre and not to the strike-slip component of the El Tigre Fault. This interpretation confirms the propagation of Quaternary deformation to the western piedmont of the Sierra del Tigre, as related to western backthrusts of this range. Considering that the minor compressive deformation develops rectilinear fault scarps on the alluvial fan terrace Q4 and Q3 developed during lower to Middle Pleistocene times (Peri *et al.,* 2018; *under review*), the tectonic propagation probably took place during Middle-Upper Pleistocene extended to Holocene (Peri *et al.*, 2018). Since the development of a bedrock fault scarp takes 500 Ka after the last fault activity, under arid climate (Burbank and Anderson, 2001), the main neotectonic event related to the piedmont deformation probably happened after the abandonment of the alluvial fan Q3, the younger terrace with fault scarps (Figures 8a and b), and before the deposition of the youngest Q2 and Q1 that do not show fault scarps.

Contributions to the partition of deformation in the western margin of Precordillera

Our results, in agreement with previous studies (Siame *et al.*, 2005, 2006), suggest that the partition of deformation is an essential tectonic process in the western margin of Precordillera at these latitudes. The Andean foreland of NW Argentina is set above the flat subduction of the Nazca

Plate beneath the South American lithosphere (Anderson *et al.*, 2007; Cahill and Isacks, 1992; Yáñez *et al.*, 2001) ongoing at a rate of about 75 mm/yr with an azimuth of N78°E (Figure 1a) (Brooks *et al.*, 2003; Kendrick *et al.*, 2003, 2006) as calculated from regional GPS survey. Siame *et al.* (2005, 2006) obtained, from fault slip vector data, that in the Western and Central Precordillera, the stress regime is mainly controlled by a σ1 parallel to that determined for the Chilean trench. These authors postulated that the subduction zone itself accommodates the convergence obliquity at the plate boundary. However, a clockwise rotation of the main stress σ1 in some strike-slip structures suggests that Pliocene-Quaternary partition of deformation may locally occur at a crustal scale in the Andean foreland. Mainly, geometry and segmentation of the El Tigre Fault and Precordillera ranges are strongly related since they show parallel trends with small changes controlled by major discontinuities (Siame *et al.*, 1997b). El Tigre Fault corresponds to a crustal-scale strike-slip fault, closely related to the Precordilleran thrust-and-fold belt, constituting a Pliocene-Quaternary transpressive system, as the former accommodates the lateral strike-slip component. In contrast, the Eastern Precordillera and the westernmost Pampean Ranges thrusts should accommodate WNW-ESE (N110°) trending shortening.

The results presented here support the idea of a local partition of deformation between the strike-slip component of the El Tigre Fault and the compressive component of the thrust and backthrust of the Sierra del Tigre, as well as in the piedmont deformation belt studied here (Figure 9). Our results also suggest that the compressive motion involving the minor piedmont deformation has happened during the Middle-Upper Pleistocene extended to the Holocene (Peri *et al.*, 2018). Moreover, the strike-slip movement of El Tigre Fault has been initiated at Pliocene (Fazzito *et al.*, 2016) continued during the Holocene (Siame *et al.,* 1997a, b), so the partition of deformation in the western margin of Precordillera is probably active during Quaternary until today.

6. CONCLUSIONS

a. ETRs models allowed us to recognize three geoelectrical levels. The more surficial and resistive level A (> 200-300 Ohm.m) shows horizontal to tilted stratification, sometimes curved geometry and it is correlated to Pleistocene alluvial fan terraces Q4 and Q3. A less resistive level B (50-300/450 Ohm.m) extends under level A with variable lateral configuration and it is correlated to the Neogene substratum constituted by the Rodeo Formation, represented by pelites of the Las

Flores Member in the north, and pyroclastic ash tuffs of the Lomas del Campanario Member at central and south areas. The conductive level C (< 30-40 Ohm.m at the north and central areas; < 250 Ohm.m at the south) is intercalated in level B and it shows horizontal disposition or irregular shapes. Level C is correlated to a porous lithology of the Rodeo Formation, represented by sandstones to conglomerates of the Las Flores Member in the north, and pyroclastic block and ash of the Lomas del Campanario Member at central and southern areas. Level C conform aquifers located between 20 and 40 m deep, which are interrupted by the presence of barriers constituted by faults.

b. The ETRs models allow us to recognize subvertical conductive zones (10-40 Ohm.m) related to abrupt changes in the lateral geometrical configuration. Both features were associated correlated to high angle (~60°-80°) reverse faults. Open anticlines and synclines that affect the Quaternary levels and the Neogene substratum were identified associated with the reverse faults.

c. Both dipole-dipole and Wenner-Schlumberger arrays result in very useful to model Quaternary or surficial geological structures and geoelectrical levels with contrasted resistivity values. We confirm that the dipole-dipole array better shows the subvertical features such as faults while the Wenner-Schlumberger array better shows the horizontal elements such as geoelectrical levels.

d. The structural model of the minor deformation study here is characterized by the main west vergence thrust fault associated with the main anticline and minor synclines, and several subordinated backthrusts of east vergence associated with anticlines. The architectural model indicates the prevalence of a compressive component of deformation of a main western vergence while the subordinated backthrusts collaborate to relieve the main tectonic deformation.

e. The results obtained and the structural style interpreted here allow us to conclude that the main piedmont thrust conforms a frontal splay of the western vergence backthrust of the Sierra del Tigre indicating a better connection to the compressive deformation component that uplifts that range instead of the strike-slip component of the El Tigre Fault. This tectonic propagation probably takes place during Middle-Upper Pleistocene to Holocene.

f. The results presented here are in agreement with previous studies that postulated the partition of deformation in the Andean foreland at a crustal level, probably until today. Our profiles evidence that piedmont compressive motions originated a minor deformation belt while the strike-slip movements are concentrated in the El Tigre Fault. These observations support the idea of local

partition of deformation in the western margin of Precordillera, probably during Quaternary until today.

7. ACKNOWLEDGMENTS

We acknowledge the Argentina Council for Scientific and Technical Research (CONICET, grants PIP 2012-2014, 112-201101-00294, and PIP 2015-2017, 112-201501-00836) for providing financial support. Careful corrections and suggestions from reviewers, which helped to improve the manuscript, are deeply appreciated and thanked.

8. REFERENCES

Abrahams, A.D. and Parsons, A.J., 1994. Geomorphology of Desert Environments. Chapman and Hall, 674 pp.

Allmendinger, R.W., Figueroa, D., Snyder, D., Beer, J., Mpodozis, C. and Isacks, B.L., 1990. Foreland shortening and crustal balancing in the Andes at 30°S latitude. Tectonics 9: 789-809.

Allmendinger, R.W. and Judge, P.A., 2014. The Argentine Precordillera: A foreland thrust belt proximal to the subducted plate. Geosphere 10: 1203-1218.

Alonso, M.S., 2011. Estratigrafía, sistemas depositacionales y aspectos composicionales del relleno neógeno de la cuenca Rodeo-Iglesia, San Juan, Argentina. PhD Thesis, Universidad de Buenos Aires (unpublished), 316 p., Buenos Aires.

Alvarado, P. and Ramos, V.A. 2011. Earthquake deformation in the northwestern Sierras Pampeanas of Argentina based on seismic waveform modelling. Journal of Geodynamics 51(4): 205-218.

Alvarado, P., Beck, S. and Zandt, G. 2007. Crustal structure of the south-central Andes Cordillera and backarc region from regional waveform modeling. Geophysical Journal International 170: 858-875.

Álvarez-Marrón, Rodríguez-Ferández, R., Heredia, N., Busquets, P., Colombo, F. and Brown, D., 2006. Neogene structures overprinting Palaeozoic thrust systems in the Andean Precordillera at 30º S latitude. Journal of the Geological Society of London 163: 949-64.

Anderson, M., Alvarado, P., Zandt, G. and Beck, S. 2007. Geometry and brittle deformation of the subducting Nazca plate, central Chile and Argentina. Geophysical Journal International 171: 419-434.

Baldis, B.A., Beresi, M., Bordonaro, L.O. and Vaca, A. 1982. Síntesis evolutiva de la Precordillera Argentina. 5° Congreso Latinoamericano de Geología Argentina, Proceedings 4: 399-445, Buenos Aires.

Basile, Y.A., 2004. Estudio geológico y geofísico del sector sur de las Lomas del Inca, provincia de San Juan. Bachelor Thesis, Universidad de Buenos Aires (unpublished), 118 p., Buenos Aires.

Bastías, H.E., 1985. Fallamiento cuaternario en laregión sismotectónica de Precordillera. PhD Thesis (unpublished), Universidad Nacional de San Juan, 160 p., San Juan.

Bastías, H.E. and Bastías, J.A., 1987. Fallamiento rumbo-deslizante en el borde oriental de los Andes entre los 32 y 26 grados de latitud sur. 10° Congreso Geológico Argentino, Proceedings 1: 207–210, Tucumán.

Bastías, H.E., Weidmann, N.E. and Pérez, A.M., 1984. Dos zonas de fallamiento Pliocuaternario en la Precordillera de San Juan. 9º Congreso Geológico Argentino, Proceedings 2: 329-341, San Carlos de Bariloche.

Bastías, H.E., Uliarte, E., Paredes, J.de D., Sanchez, A., Bastías, J.A., Ruzycki, L. and Perucca, P., 1990. Neotectónica de la provincia de San Juan. 11° Congreso Geológico Argentino, Relatorio de geología y recursos naturales de la Provincia de San Juan: 228-244, San Juan.

Beer, J.A., Allmendinger, R.W., Figueroa, D.A. and Jordan, T.E., 1990. Seismic stratigraphy of a Neogene piggy-back basin, Argentina. American Association of Petroleum Geology Bulletin 74: 1183-1202.

Brooks, B., Bevis, M., Smalley Jr., R., Kendrick, E., Manceda, R., Lauría, E., Maturana, R. and Araujo, M., 2003. Crustal motion in the Southern Andes (26°–36°S): Do the Andes behave like a microplate? Geochemistry, Geophysics, Geosystems 4 (10): http://dx.doi.org/10.1029/2003GC000505.

Bufford, K.M., Atekwana, E.A., Abdelsalam, M.G., Shemang, E., Atekwana, E.A., Mickus and K., Molwalefhe, L. 2012. Geometry and faults tectonic activity of the Okavango Rift Zone, Botswana: Evidence from magnetotelluric and electrical resistivity tomography imaging. Journal of African Earth Sciences 65: 61-71.

Burbank D.W. and Anderson, R.S., 2001. Tectonic geomorphology. Blackwell Science (Ed), USA: 273 pp.

Cahill, T.A. and Isacks, B.L. 1992. Seismicity and shape of the subducted Nazca Plate. Journal of Geophysical Research 97: 17503-17529.

Caputo, R., Piscitelli, S., Oliveto, A., Rizzo, E. and Lapenna, V. 2003. The use of electrical resistivity tomographies in active tectonics: examples from Tyrnavos Basin, Greece. Journal of Geodynamics 36: 19-35.

Caputo, R., Salviulo, L., Piscitelli, S. and Loperte, A., 2007. Late Quaternary activity along the Scorciabuoi Fault (Southern Italy) as inferred from electrical resistivity tomographies.

Cardó, R. and Díaz, I.N., 2005. Memoria Hoja Geológica 3169-I, Rodeo. Servicio Geológico Minero Argentino, 52 p., Buenos Aires.

Casa, A., Yamin, M., Cegarra, M., Wright, E., Coppolecchia, M., Costa, C. and García, V., 2014. Actualización del SIG de las deformaciones cuaternarias de la República Argentina. In XIX Congreso Geológico Argentino, Junio, Córdoba. Geología Estructural y Geotectónica (pp. T6-T7).

Christenson, G.E. and Purcell, C., 1985. Correlation and age of Quaternary alluvial-fan sequences, Basin and Range province, southwestern United States. Geological Society of America Special Papers 203: 115–122.

Coggon, J., 1973. A comparison of IP electrode arrays. Geophysics 38(4): 737-761.

Colella, A., Lapenna, V. and Rizzo, E. 2004. High-resolution imaging of the High Agri Valley Basin (Southern Italy) with electrical resistivity tomography. Tectonophysics 386: 29-40.

Cortés, J.M. and Cegarra, M., 2004. Plegamiento cuaternario transpresivo en el piedemonte suroccidental de la Precordillera sanjuanina. In: Cortés, J.M., Rossello, E.A., Dalla Salda, LH. (eds), Avances en Microtectónica. Asociación Geológica Argentina, Serie D, Publicación Especial 7: 68-75, Buenos Aires.

Cortés, J.M., Vinciguerra, P., Yamín, M. and Pasini, M.M., 1999. Tectónica Cuaternaria de la Región Andina del Nuevo Cuyo (28°- 38° LS). In: Caminos, R. (ed.), Geología Argentina. Subsecretaría de Minería de la Nación, Servicio Geológico Minero Argentino, Analls 29: 760-778, Buenos Aires.

Cortés, J.M., Pasini, M. and Yamin, M., 2005a. Paleotectonic controls on the distribution of Quaternary deformation in the southern Precordillera, Central Andes (31°30'-33° SL). 6th International Symposium on Andean Geodynamics: 186-189, Barcelona.

Cortés, J.M., Yamín, M.G., and Pasini, M.M., 2005b. La Precordillera Sur, Provincias de Mendoza y San Juan. 16º Congreso Geológico Argentino, Actas 1: 395-402, La Plata.

Cortés, J.M., Casa, A., Pasini, M.M., and Yamin, M.G., 2005c. Fajas de estructuras neotectónicas asociadas a rasgos paleotectónicos en Precordillera y Cordillera Frontal (31º30'-33º30'LS). 16º Congreso Geológico Argentino, Actas 4: 463-466, La Plata.

Cortés, J.M., Casa, A., Pasini, M.M., Yamin, M.G. and Terrizzano, C., 2006. Fajas oblicuas de deformación neotectónica en Precordillera y Cordillera Frontal (31°30'–33°30' LS). Controles paleotectónicos. Revista de la Asociación Geológica Argentina 61: 639-646.

Cortés, J.M., Casa, A.L., Yamin, M.G., Pasini, M. and Terrizzano, C.M., 2014. Unidades morfotectónicas, estructuras oblicuas y patrones de distribucinón de la deforamción cuaternarias en la Precordillera de Cuyo (28°-33°S). 19° Congreso Geológico Argentino, Actas: S20-14, Córdoba.

Cortes, J.M., Terrizzano, C.M., Pasini, M.M., Yamin, M.G. and Casa, A.L., 2015. Quaternary tectonics along oblique deformation zones in the Central Andean retro-wedge between 31° 30' S and 35° S. Geological Society, London, Special Publications 399 (1): 267-292.

Costa, C., Diederix, H., Gardini, C. and Cortés, J., 2000a. The Andean orogenic front at Sierra de Las Peñas-Las Higueras, Mendoza, Argentina. Journal of South American Earth Sciences 13: 287-292.

Costa, C., Gardini, C. and Diederix, H., 2000b. The Montecito anticline: A Quaternary growing structure in the Precordilleran foothills of northern Mendoza. Argentina, presented at the 9th Congreso Geológico Chileno. 758–762.

Costa, C.H., Audemard M., F.A., Bezerra, F.H.R., Lavenu, A., Machette, M.N. and París, G. 2006. An Overview of the Main Quaternary Deformation of South America. Revista de la Asociación Geológica Argentina 61: 461-479.

Costa, C.H., Ahumada, E.A., Vázquez, F.R. and Kröhling, D.M., 2015a. Holocene shortening rates of an Andean-front thrust, Southern Precordillera, Argentina. Tectonophysics 664: 191-201.

Costa, C., Ahumada, E., Gardini, C., Vazquez, F. and Diederix, H., 2015b. Quaternary shortening at the orogenic front of the Central Andes of Argentina (32°15'–32°40'S): A field survey of the Las Peñas thrust. In: Sepúlveda, S., Giambiagi, L., Moreiras, S., Pinto, L., Tunik, M., Hoke, G., Farías, M. (Eds.), Geodynamic processes in the Andes of Central Chile and Argentina. Geological Society Special Publication 399.

Cristallini, E.O. and Ramos, V.A., 2000. Thick-skinned and thin-skinned thrusting in La Ramada fold and thrust belt: crustal evolution of the high Andes of San Juan, Argentina (32° SL). Tectonophysics 317: 205-235.

Fazzito, S.Y., Rapalini, A.E., Cortés, J.M. and Terrizzano, C.M. 2009. Characterization of Quaternary Faults by Electric Resistivity Tomography in the Andean Precordillera of Western Argentina. Journal of South American Earth Sciences 28: 217-228.

Fazzito, S. Y., Cortés, J. M., Rapalini, A. E. and Terrizzano, C.M. 2013. The geometry of the active strike-slip El Tigre Fault, Precordillera of San Juan, Central–Western Argentina: integrating resistivity surveys with structural and geomorphological data. International Journal of Earth Sciences 102: 1447-1466.

Fazzito, S.Y., Rapalini, A.E., Cortés, J.M. and Terrizzano, C.M. 2016. Vertical-axis rotations and deformation along the active strike-slip El Tigre Fault (Precordillera of San Juan, Argentina) assessed through palaeomagnetism and anisotropy of magnetic susceptibility. International Journal of Earth Sciences: doi: 10.1007/s00531-016-1332-1.

Furque, G. 1979. Descripción geológica de la Hoja 18c, Jáchal. Provincia de San Juan. Servicio Geológico Nacional, Bulletin 164, 79 p., Buenos Aires.

Giambiagi, L. and Ramos, V., 2002. Structural evolution of the Andes in a transitional zone between flat and normal subduction (33°30'–33°45'S), Argentina and Chile. Journal of South American Earth Sciences 15 (1): 101–116.

Gutscher, M.A., Spakman, W., Bijwaard, H. and Engdahl, E.R. 2000. Geodynamics of flat slab subduction: seismicity and tomographic constraints from the Andean margin. Tectonics 19: 814-833.

Hooke, R.L., 1967. Processes on arid region alluvial fans. Journal of Geology 75(4): 438–460.

INPRES 1982. Microzonificación sísmica del valle de Tulúm, provincia de San Juan. Instituto Nacional de Prevención Sísmica. Resumen Ejecutivo, San Juan.

Johnson, A. T., Jordan, T.E., Johnson, N.M., and Naeser, C., 1987. Cronología y velocidad de sedimentación en una secuencia volcaniclástica, Rodeo, Prov. de San Juan, Rep. Argentina. 10° Congreso Geológico Argentino, Proceedings 2: 87-90, Tucumán.

Jordan, T.E., Allmendinger, R.W., Damanti, J.F. and Drake, R., 1993. Chronology of motion in a complete thrust belt: the Precordillera, 30–31º S, Andes Mountains. Journal of Geology 101: 135-156.

Kendrick, E., Bevis, M., Smalley Jr., R., Brooks, B., Vargas, R., Lauría, E. and Fortes, L., 2003. The Nazca-south America Euler vector and its rate of change. Journal of South American Earth Sciences 16: 125-131.

Kendrick, E., Brooks, B., Bevis, M., Smalley Jr., R., Lauria, E., Araujo, M. and Parra, H., 2006. Active orogeny of the South-Central Andes studied with GPS geodesy. Revista Asociación Geológica Argentina 61 (4): 555–566.

Levina, M., Horton, B.K., Fuentes, F. and Stockli, D.F., 2014. Cenozoic sedimentation and exhumation of the foreland basin system preserved in the Precordillera thrust belt (31-32S), southern central Andes, Argentina. Tectonics 33: 1659-1680. http://dx.doi.org/10.1002/2013TC003424.

Loke, M.H., 1996-2015. Tutorial: 2-D and 3-D electrical imaging surveys. Geotomo Software.

Loke, M.H. and Barker, R.D., 1996. Rapid least-squares inversion of apparent resistivity pseudosections by a quasi-Newton method 1. Geophysical prospecting 44(1): 131-152.

Loke, M.H., Acworth, I. and Dahlin, T., 2003. A comparison of smooth and blocky inversion methods in 2D electrical imaging surveys. Exploration Geophysics 34(3): 182-187.

Ludwiniak, M., Śmigielski, M., Kowalczyk, S., Łoziński, M., Czarniecka, U. and Lewińska, L., 2019. The intramontane Orava Basin–evidence of large-scale Miocene to Quaternary sinistral wrenching in the Alpine-Carpathian-Pannonian area. Acta Geologica Polonica: 1-48.

Meigs, A., Krugh, W., Schiffman, C., Vergés, J. and Ramos, V., 2006. Refolding of thin-skinned thrust sheets by active basement-involved thrust faults in the eastern Precordillera of western Argentina. Revista Asociación Geológica Argentina 61 (4): 589–603.

Nguyen, F., Garambois, S., Jongmans, D., Pirard, E. and Loke, M.H. 2005. Image processing of 2D resistivity data for imaging faults. Journal of Applied Geophysics 57: 260-277.

Nguyen, F., Garambois, S., Chardon, D., Hermitte, D., Bellier, O. and Jongmans, D., 2007. Subsurface electrical imaging of anisotropic formations affected by a slow active reverse fault, Provence, France. Journal of applied geophysics 62(4): 338-353.

Nivière, B., Bruestle, A., Bertrand, G., Behermann, J. and Gourry, J.C., 2008. Active tectonics of the south-eastern Upper Rhine Graben, Freiburg area (Germany). Quaternary Science Reviews 27: 541-555.

Ortiz, A. and Zambrano, J. 1981. La provincia geológica de Precordillera Oriental. 8° Congreso Geológico Argentino, Proceedings 3: 59-74, San Luis.

Pánek, T., Táborík, P., Klimeš, J., Komárková, V., Hradecký, J. and Šťastný, M.., 2011. Deep-seated gravitational slope deformations in the highest parts of the Czech Flysch Carpathians:

evolutionary model based on kinematic analysis, electrical imaging and trenching. Geomorphology 129(1–2): 92-112.

Pérez, P., 2018. Estudios neotectónicos y geofísicos en la zona de la Falla El Tigre, San Juan. Master Thesis (unpublished), Universidad de Buenos Aires, 95 pp.

Pérez, I. and Costa, C., 2011. El braquianticlinal del Cerro Negro de Iglesia y su relación con el Sistema de Fallamiento El Tigre, provincia de San Juan, Argentina. 18° Congreso Geológico Argentino, Proceedings in CD. doi: 10.13140/RG.2.1.3337.8409.

Peri, V.G., Fazzito, S.Y., Bello Camilletti, G., Rapalini, A.E. and Cortés, J.M., 2017. Estudios geoeléctricos de subsuelo sobre estructuras vinculadas a la Falla El Tigre, San Juan. Revista de la Asociación Geológica Argentina 74(4): 468-484.

Peri, G., Haghipour, N., Terrizzano, C., Cortés, J.M., Yamin, M., Perez, P. and Burg, J-P., 2018. Control tectónico y climático en la evolución del paisaje en el margen Occidental de la Precordillera Sanjuanina, Argentina. VII Congreso Argentino de Cuaternario y Geomorfología, 18 al 21 de Septiembre de 2018, Naturalia Patagónica (10), Aostracts: 189-190, Puerto Madryn.

Peri, G., Haghipour, N., Christl, M., Terrizzano, C., Kaveh, A., Yamin, M., Klinger, F., Pérez, P., Barcelona, H., and Burg, J-P. (under review in Quaternary Science Reviews). Tectonic and climatic control on Quaternary landscape evolution at the western margin of Precordillera Argentina, constrained by cosmogenic dating (^{10}Be).

Perucca, L.P. and Martos, L.M., 2008. Análisis preliminar de la evolución del paisaje cuaternario en el valle de Iglesia, San Juan. Revista de la Asociación Geológica Argentina 65: 624-637.

Perucca, L.P. and Martos, L.M., 2012. Geomorphology, tectonism and Quaternary landscape evolution of the central Andes of San Juan (30° S–69° W), Argentina. Quaternary international 253: 80-90.

Petrit, K., Klamthim, P. and Duerrast, H., 2018. 3D resistivity survey for shallow subsurface fault investigations. In E3S Web of Conferences, Volume 34: p. 01007, EDP Sciences.

Ramos, V.A., 2009. Anatomy and global context of the Andes: Main geologic features and the Andean orogenic cycle. Geological Society of America, Memoir 204: 31-65.

Ramos, V.A., Vujovich, G.I. and Dallmeyer, R.D. 1996. Los klippes y ventanas tectónicas de la estructura perándica de la Sierra de Pie de Palo (San Juan): edad e implicaciones tectónicas. 18° Congreso Geológico Argentino y 3° Congreso Exploración de Hidrocarburos, Proceedings 5: 377-392, Buenos Aires.

Ramos, V.A., Cristallini, E.O. and Perez, D.J. 2002. The Pampean flat-slab of the central Andes. Journal of South American Earth Sciences 15: 59-78.

Ramos, V., Zapata, T., Cristallini, E. and Introcaso, A., 2004. The Andean thrust system - Latitudinal variations in structural styles and orogenic shortening. American Association of Petroleum Geologists Memories 82: 30–50.

Rizzo, E. and Giampaolo, V., 2019. New deep electrical resistivity tomography in the High Agri Valley basin (Basilicata, Southern Italy). Geomatics, Natural Hazards and Risk 10(1): 197-218.

Rizzo, E., Colella, A., Lapenna, V. and Piscitelli, S., 2004. High-resolution images of the fault-controlled High Agri Valley basin (Southern Italy) with deep and shallow electrical resistivity tomographies. Physics and Chemistry of the Earth, Parts A/B/C 29(4-9): 321-327.

Rockwell, T., Ragona, D., Meigs, A., Owen, L., Costa, C. and Almeda, E., 2014. Inferring a thrust-related earthquake history from secondary faulting: A long rupture record of La Laja Fault, San Juan, Argentina. Bull. Seismological Society of America 104 (1), 269–284. http:// dx.doi.org/10.1785/0120110080.

Schmidt, S., Hetzel, R., Mingorance, F. and Ramos, V., 2011. Coseismic displacements and Holocene slip rates for two active thrust faults at the mountain front of the Andean Precordillera (~33°S). Tectonics 30, TC5011. http://dx.doi.org/10.1029/ 2011TC002932.

Sharma, P.S., 1997. Enviromental and Engineering Geophysics. Cambridge University Press.

Siame, L.L., 1998. Cosmonucléide produit in-situ (^{10}Be) et quantification de la déformation active dans les Andes centrales. These de doctorat. Université de Paris-Sud, Orsay, France.

Siame, L.L., Bourles, D.L, Sebrier, M., Bellier, O., Castano, J.C., Araujo, M., Perez, M., Raisbeck, G.M. and Yiou, F., 1997a. Cosmogenic dating ranging from 20 to 700 ka of a series of alluvial fan surfaces affected by the El Tigre Fault, Argentina. Geology 25: 975-978.

Siame, L.L., Sébrier, M., Bellier, O., Bourlès, D.L., Castaño, J.C. and Araujo, M., 1997b. Geometry, segmentation and displacement rates of the El Tigre Fault, San Juan Province (Argentina) from SPOT image analysis and 10Be datings. Annales Tectonicae 1: 3-26.

Siame, L., Bellier, O., Sébrier, M., Bourlès, D., Leturmy, P., Perez, M. and Araujo, M., 2002. Seismic hazard reappraisal from combined structural geology, geomorphology and cosmic ray exposure dating analyses: the Eastern Precordillera thrust system (NW Argentina). Geophysical Journal International 150 (1): 241–260. http://dx.doi.org/10.1046/j.1365-246X.2002.01701.x.

Siame, L.L., Bellier, O., Sebrier, M. and Araujo, M. 2005. Deformation partitioning in flan subduction setting: case of the Andean foreland of western Argentina (28°S–33° S). Tectonics 24: 1-24.

Siame, L.L., Bellier, O. and Sebrier, 2006. Active tectonics in the Argentine Precordillera and western Sierras Pampeanas. Revista de la Asociación Geológica Argentina 61: 604-619.

Smalley, R.F. and Isacks, B.L., 1987. A high-resolution local network study of the Nazca Plate Wadati-Benioff Zone under western Argentina. Journal of Geophysical Research: Solid Earth 92(B13): 13903-13912.

Smalley Jr,R. and Isacks, B.L., 1990. Seismotectonics of thin-and thick-skinned deformation in the Andean Foreland from local network data: Evidence for a seismogenic lower crust. Journal of Geophysical Research: Solid Earth 95(B8): 12487-12498.

Smalley Jr,R., Pujol, J., Regnier, M., Chiu, J.M., Chatelain, J.L., Isacks, B.L., Araujo, M. and Puebla, N., 1993. Basement seismicity beneath the Andean Precordillera thin-skinned thrust belt and implications for crustal and lithospheric behavior. Tectonics 12(1): 63-76.

Staley, J.T., Adams, J.B. and Palmer, F.E., 1991. Desert varnish: a biological perspective. In: Stotzky, G. and Bollag, J. (Eds.), Soil Biochemistry, Volume 7: 173-195.

Suriano, J., Mardonez, D., Mahoney, J. B., Mescua, J. F., Giambiagi, L. B., Kimbrough, D. and Lossada, A., 2017. Uplift sequence of the Andes at 30° S: Insights from sedimentology and U/Pb dating of synorogenic deposits. Journal of South American Earth Sciences 75: 11-34.

Targa, D.A., Moreira, C.A., Camarero, P.L., Casagrande, M.F.S. and Alberti, H.L.C., 2019. Structural analysis and geophysical survey for hydrogeological diagnosis in uranium mine, Poços de Caldas (Brazil). SN Applied Sciences 1(4): 299.

Telford, W.M., Geldart, L.P. and Sheriff, R.E., 1990. Applied Geophysics, second ed. Cambridge University Press, Cambridge, UK, 790 pp.

Terrizzano, C.M., Fazzito, S.Y., Cortés, J.M. and Rapalini, A.E. 2010. Studies of Quaternary deformation zones through geomorphic and geophysical evidence: A case in the Precordillera Sur, Central Andes of Argentina. Tectonophysics 490: 184-196.

Terrizzano, C.M., Fazzito, S.Y., Cortés, J.M. and Rapalini, A.E., 2012. Electrical resistivity tomography applied to the study of neotectonic structures, northwestern Precordillera Sur, Central Andes of Argentina. Journal of South American Earth Sciences 34: 47-60.

Terrizzano, C. M., Cortés, J. M., Zech, R. and Morabito, E.G., 2014. Drainage anomalies as indicators of soft-linked deformation zones between neotectonic structural highs in the Precordillera, Central Andes of Argentina. Geomorphology 224: 1-15.

Vallejo, M.D., 2004. Estudio geológico y geofísico del sector norte de Lomas del Inca, Barreal del Leoncito, San Juan. Bachelor Thesis, Universidad de Buenos Aires (unpublished), 120 p., Buenos Aires.

Vergés, J., Ramos, V., Meigs, A., Cristallini, E., Bettini, F. and Cortés, J., 2007. Crustal wedging triggering recent deformation in the Andean Thrust front between 31°S and 33°S: Sierras Pampeanas-Precordillera interaction. Journal of Geophysical Research 112, B03S15. http://dx.doi.org/10.1029/2006JB004287.

von Gosen, W., 1992. Structural evolution of the Argentine Precordillera: the Río San Juan section. Journal of Structural Geology 14: 643- 667.

Walcek, A.A. and Hoke, G.D., 2012. Surface uplift and erosion of the southernmost Argentine Precordillera. Geomorphology 153: 156-168. http://dx.doi.org/10.1016/j.geomorph.2012.02.021.

Wetten, C., 1975 a. Geología del valle de Iglesia, su relación con los yacimientos de diatomita de Lomas del Campanario e importancia económica. Master Thesis (unpublished),, Universidad Nacional de San Juan, 70 p.

Wetten, C., 1975 b. Estudio geológico económico de un yacimiento de diatomita y análisis de mercado. Proceedings 2° Congreso Iberoamericano de Geología Económica 5: 513 - 529. Argentina.

Wise, D.J., Cassidy, J. and Locke, C.A., 2003. Geophysical imaging of the quaternary Wairoa North Fault, New Zealand: a case study. Journal of Applied Geophysics 53(1): 1-16.

Yamin, M.G., 2007. Neotectónica del bloque Barreal, margen noroccidental de la Precordillera Sur. PhD Thesis, Universidad de Buenos Aires (unpublished), 230 p., Buenos Aires.

Yáñez, G. A., Ranero, C. R., von Huene, R., and Díaz, J., 2001. Magnetic anomaly interpretation across the southern central Andes (32–34 S): The role of the Juan Fernández Ridge in the late Tertiary evolution of the margin. Journal of Geophysical Research: Solid Earth 106(B4): 6325-6345.

Zapata, T. and Allmendinger, R., 1996. Thrust front zone of the Precordillera, Argentina: a thick-skinned triangle zone. Bulletin of American Association of Petroleum Geologists 80: 359–381.

V. Gisel Peri: Conceptualization, Writing, Original draft preparation, Methodology, Data acquisition and processing, Reviewing and Editing. **Augusto E. Rapalini:** Investigation, Supervision, Methodology, Data acquisition, Writing, Reviewing and Editing. **Pablo Pérez:** Investigation, Methodology, Data acquisition. **Pablo Franceschinis:** Data acquisition, Reviewing and Editing. **M. Flavia Leiva:** Data processing, Reviewing and Editing. **Sabrina Fazzito:** Methodology, Data processing, Validation. **José M. Cortés:** Investigation, Supervision, Writing, Reviewing and Editing.

Declaration of interests

☒ The authors declare that they have no known competing financial interests or personal relationships that could have appeared to influence the work reported in this paper.

☐The authors declare the following financial interests/personal relationships which may be considered as potential competing interests:

HIGHLIGHTS

6. Quaternary analysis of the western piedmont of Sierra del Tigre is presented.
7. Topographic and geoelectrical surveys were done across fault and fold scarps.
8. Three geoelectrical levels and subvertical conductive zones were identified.
9. A frontal splay of the backthrust of the Sierra del Tigre was inferred.
10. Quaternay compressive deformation has originated the piedmont deformation belt.